



Arabidopsis PROTODERMAL FACTOR2 binds lysophosphatidylcholines and transcriptionally regulates phospholipid metabolism

Izabela Wojciechowska¹, Thiya Mukherjee^{2,3,4}, Patrick Knox-Brown⁵, Xueyun Hu^{2,6}, Aashima Khosla^{2,3} , Bibek Subedi^{2,3} , Bilal Ahmad^{2,3} , Graham L. Mathews², Ashley A. Panagakis², Kyle A. Thompson², Sophie T. Peery², Jagoda Szlachetko¹, Anja Thalhammer⁵, Dirk K. Hincha^{1*}, Aleksandra Skirvcz^{1,7} and Kathrin Schrick^{2,3}

1 Max Planck Institute of Molecular Plant Physiology, 14476, Potsdam, Germany; 2 Division of Biology, Kansas State University, Manhattan, KS 66506, USA; 3 Molecular, Cellular and Developmental Biology, Kansas State University, Manhattan, KS 66506, USA; 4Donald Danforth Plant Science Center, Olivette, MO 63132, USA; 5Physical Biochemistry, University of Potsdam, 14476, Potsdam, Germany; ⁶Joint International Research Laboratory of Agriculture and Agri-Product Safety of Ministry of Education of China, Yangzhou University, Yangzhou, 225009, China; ⁷Department of Biochemistry and Molecular Biology, Michigan State University, East Lansing, MI 48823, USA

Authors for correspondence: Kathrin Schrick Email: kschrick@ksu.edu

Aleksandra Skirvcz Email: skirycza@msu.edu

Received: 14 January 2024 Accepted: 6 May 2024

New Phytologist (2024) doi: 10.1111/nph.19917

Key words: Arabidopsis, HD-Zip IV transcription factors, lipidomics, lysophospholipids, phosphate, START domain.

Summary

- Plant homeodomain leucine zipper IV (HD-Zip IV) transcription factors (TFs) contain an evolutionarily conserved steroidogenic acute regulatory protein (StAR)-related lipid transfer (START) domain. While the START domain is required for TF activity, its presumed role as a lipid sensor is not clear.
- Here we used tandem affinity purification from Arabidopsis cell cultures to demonstrate that PROTODERMAL FACTOR2 (PDF2), a representative member that controls epidermal differentiation, recruits lysophosphatidylcholines (LysoPCs) in a START-dependent manner. Microscale thermophoresis assays confirmed that a missense mutation in a predicted ligand contact site reduces lysophospholipid binding.
- · We additionally found that PDF2 acts as a transcriptional regulator of phospholipid- and phosphate (Pi) starvation-related genes and binds to a palindromic octamer with consensus to a Pi response element. Phospholipid homeostasis and elongation growth were altered in pdf2 mutants according to Pi availability. Cycloheximide chase experiments revealed a role for START in maintaining protein levels, and Pi starvation resulted in enhanced protein destabilization, suggesting a mechanism by which lipid binding controls TF activity.
- We propose that the START domain serves as a molecular sensor for membrane phospholipid status in the epidermis. Our data provide insights toward understanding how the lipid metabolome integrates Pi availability with gene expression.

Introduction

Interactions between proteins and lipids are dynamic in living organisms, yet the full extent and biological significance of such interactions is underexplored, especially in plants. In Arabidopsis thaliana (hereafter Arabidopsis), 16 homeodomain leucine zipper transcription factors of the class IV family (HD-Zip IV TFs) contain a lipid sensor called the START domain (Schrick et al., 2004). Steroidogenic acute regulatory protein (StAR)-related lipid transfer (START) domains were first characterized in mammalian proteins involved in lipid transfer, metabolism and sensing (Ponting & Aravind, 1999; Alpy & Tomasetto, 2005). In humans, the START domain is found in 15 proteins, several of which are known to

bind specific sterols, bile acids, phospholipids, sphingolipids, or steroid hormones (Alpy et al., 2009; Letourneau et al., 2012, 2015; Clark, 2020). Homology modeling of START domains from Arabidopsis HD-Zip IV TFs suggests that plant proteins contain a similar ligand-binding pocket (Schrick et al., 2014). In accordance, deletion of this domain from HD-Zip IV member GLABRA2 (GL2) results in loss-of-function phenotypes that are partially complemented by the START domain from mammalian STARD1/StAR (Schrick et al., 2014). The observed complementation is abolished by a binding-site mutation, implying importance of lipid binding for GL2 function. Moreover, START domains from HD-Zip IV TFs PROTODERMAL FACTOR2 (PDF2) and Arabidopsis thaliana MERISTEM LAYER1 (ATML), promote transcriptional activity of a chimeric TF in yeast (Schrick et al., 2014).

^{*}Dedicated to the memory of our colleague and friend Dirk K. Hincha.

PDF2 and its paralog ATML1 are thought to be functionally redundant and play a critical role in maintenance of epidermal (L1) identity of the vegetative, floral and inflorescence shoot apical meristem (Abe et al., 2003). Double knockout mutants of PDF2 and ATML1 result in severe defects in shoot epidermal cell differentiation, leading to embryonic lethality (Ogawa et al., 2015), while overexpression of ATML1 is sufficient to induce epidermal identity in internal cell layers (Takada et al., 2013). Moreover, double mutants of PDF2 with other family members (HDG1, HDG2, HDG5, HDG12), result in floral organ defects (Kamata et al., 2013a). ATML1 and PDF2 TFs bind to the L1 box, a promoter element specific to L1 genes such as those coding for extracellular proline-rich protein PROTODERMAL FACTOR1 (PDF1) (Abe et al., 2003), GDSL lipase LIP1 (Rombola-Caldentey et al., 2014) and ketoacyl-CoA synthase (KCS20), the latter of which catalyzes very long chain fatty acid (VLCFA) biosynthesis (Rombola-Caldentey et al., 2014). VLCFA produced in the epidermis are thought to function as signals affecting proliferation of internal tissues via inhibition of cytokinin synthesis, thus modulating plant growth (Nobusawa et al., 2013). PDF2 and ATML1 are reported to interact with DELLA proteins in regulation of cell expansion (Rombola-Caldentey et al., 2014). Upon gibberellin accumulation, DELLAs are subjected to proteolysis, releasing PDF2 and ATML1 to activate expression of L1 genes (Rombola-Caldentey et al., 2014).

Considering the key role of PDF2 and ATML1 in epidermal development, we investigated additional layers of regulation, whereby TF activity is controlled by a small molecule ligand. Based on the presence of an evolutionary conserved lipid-binding domain and their role as developmental regulators, plant HD-Zip START-containing TFs were suggested to constitute a link between lipid metabolism and plant development (Ponting & Aravind, 1999; Schrick et al., 2004). We hypothesized that START, by binding lipids, controls gene expression analogously to nuclear receptors from animals. An advantage of such a mechanism is that the metabolic states could be linked to cell growth and differentiation. However, the identities of small molecule ligands that bind the START domain in planta have remained elusive. To address this gap in knowledge, we applied a tandem affinity purification protocol using Arabidopsis cell cultures for analysis of small molecule partners of PDF2, a representative HD-Zip IV TF. We then performed an in vitro assay that indicates direct binding of START to lysophosphatidylcholines. Genetic analysis suggests that PDF2 TF function is critical to regulate the expression of several phospholipid and phosphate starvation response genes, and its levels are important for lipid composition. We propose a role for PDF2 in sensing membrane phospholipid status via its START domain.

Materials and Methods

Plant cell cultures, plants and growth conditions

PSB *Arabidopsis thaliana* cell cultures (Van Leene *et al.*, 2011) were grown in MSMO medium with 3% sucrose, 0.05 mg l^{-1} kinetin and 0.5 mg l^{-1} 1-naphthaleneacetic acid on a shaker. Cells were

passaged weekly to fresh medium and harvested during logarithmic growth using rapid filtration and liquid nitrogen snap freezing. Transformation with TAP constructs was as described previously (Van Leene et al., 2011). Arabidopsis thaliana plants were of the Columbia (Col-0) ecotype. Seeds for pdf2-1 and atml1-1 (Abe et al., 2003) were provided by Taku Takahashi. Both atml1-3 (SALK_033408) and atml1-4 (SALK_128172) are T-DNA insertion alleles (Roeder et al., 2012) provided by Adrienne Roeder. gl2-5 is a En-1 insertion allele of GL2 (Ohashi et al., 2003; Khosla et al., 2014). pdf2-2 (SALK_109425) and pdf2-4 (SAIL_70G06) T-DNA insertion lines (Peterson et al., 2013; Kamata et al., 2013b; San-Bento et al., 2014) were from ABRC. Genotyping primers are listed in Supporting Information Table S1. HA: PDF2 and HA:GL2 were transformed into Col-0 plants. The proGL2:EYFP:GL2, proGL2:EYFP:PDF2 and proGL2:EYFP:PDF2 constructs (and mutant variants) were transformed into gl2-5, while proGL2:EYFP:PDF2 was additionally transformed into ATML1/atml1-1;pdf2-1 and Col-0. Agrobacterium strain GV3101 (MP90) was used for transformation and construction of transgenics by floral dip (Clough & Bent, 1998), followed by selection on 20 µg ml⁻¹ hygromycin B. Segregation patterns of 3:1 for EYFP expression were observed among T2 progeny from at least 20 independent transformants, and representative homozygous T3 lines were selected for analysis. Plants were grown at 23°C under continuous light on soil comprised of Metro-Mix 380, vermiculite and perlite (4:3:2) (Hummert International). For RNA or lipid extraction, seeds were sterilized by chlorine gas treatment and sown onto 0.8% agar (Micropropagation Type II; Caisson Labs, Smithfield, UT, USA) containing Murashige & Skoog (MS) basal salts (Sigma-Aldrich) (Murashige & Skoog, 1962), 1% Suc, and 0.05% MES buffer at pH 5.8. Seeds were transferred to 23°C and grown under continuous light for 12 or 14 d. A razor blade was used to remove roots, and shoots were processed for RNA or lipid extraction. For growth under Pi limitation, vapor-sterilized seeds were germinated on Pi sufficient (P+) media (20.6 mM NH₄NO₃, 2.26 mM CaCl₂ dihydrate, 0.759 mM MgSO₄ heptahydrate, 18.8 mM KNO₃ and 1.25 mM KH₂PO₄ monobasic, MS micronutrient solution (M529, PhytoTech Labs, Lenexa, KS, USA), 1% Suc, 0.05% MES, pH 5.7, 0.8% agar) or Pi limiting (P-) media (lacking KH₂PO₄ monobasic).

Constructs for plant transformation

Tandem affinity purification constructs were generated by Gateway technology using *pKCTAP* and *pKNGSTAP* as described previously (Van Leene *et al.*, 2011). PDF2 was amplified from an *Arabidopsis* cDNA library using PCR primers listed in Table S1. The pdf2^{ASTART} constructs were generated by PCR amplification of PDF2 binary N' and C' TAP constructs using PCR primers flanking the START domain (Table S1) followed by ligation. The SR54 binary vector for expression of GL2 under its native promoter (*proGL2:EYFP:GL2*) was previously described (Schrick *et al.*, 2014). To construct binary vectors expressing *PDF2* and *ATML1*, cDNA sequences were PCR amplified using Q5 High Fidelity Polymerase (New England Biolabs, Ipswich, MA, USA) and cloned into SR54 *proGL2:EYFP* cleaved with *Sall* and *KpnI*

using NEBuilder HiFi DNA Assembly Master Mix (New England Biolabs) with gene-specific primers (Table S1). The ΔSTART (ΔST) and K107E mutations in *PDF2* were generated using the Q5 Site-Directed Mutagenesis Kit (New England Biolabs) (Mukherjee *et al.*, 2022). The L480P mutation in *GL2* was generated by one-step PCR-based site-directed mutagenesis (Scott *et al.*, 2002) using PfuUltra II Fusion HS DNA polymerase (Agilent Technologies) with primers listed in Table S1. *HA: PDF2* and *HA:GL2* were constructed by transferring the respective cDNAs from pENTR/D-TOPO plasmids into pEarleyGate 201 (Earley *et al.*, 2006) using Gateway LR Clonase II (Invitrogen).

Tandem affinity purification

Affinity purification was performed as previously described (Luzarowski et al., 2017, 2018). Whole cell native protein lysates (inputs) were harvested from Arabidopsis cell cultures expressing 35S:TAP:PDF2, 35S:PDF2:TAP, 35S:TAP:pdf2^{\Delta START}, 35S: pdf2^{\Delta START}:TAP, or empty vector. A soluble (membrane depleted) fraction was obtained by centrifugation of the lysate for 10 min at 14 000 rcf at 4°C, followed by ultracentrifugation for 1 h at 35 000 rcf at 4°C, and subsequent incubation with IgG Sepharose. After stringent washes, bait proteins were released from the beads by TEV protease cleavage. Samples were extracted as previously described (Giavalisco et al., 2011), using a methyltert-butyl ether (MTBE)/methanol/water solvent system to separate proteins, lipids, and polar compounds into pellet, organic, and aqueous phases, respectively. Following extraction, organic and aqueous phases were dried and stored at -20°C until LC/MS analysis.

LC/MS analysis

Ultra-performance liquid chromatography (Waters Acquity UPLC System, Milford, MA, USA) coupled to an Exactive mass spectrometer (Thermo Fisher Scientific, Waltham, MA, USA) in positive and negative ionization mode was used to analyze the samples as described (Giavalisco et al., 2011). UPLC separation of the polar fraction was performed using an HSS T3 C18 reversed-phase column (100 mm × 2.1 mm × 1.8 μm particles; Waters). The mobile phases were 0.1% formic acid in water (Buffer A, ULC/MS; Biosolve, Dracut, MA, USA) and 0.1% formic acid in acetonitrile (Buffer B, ULC/MS; Biosolve). A 2 μl sample (the dried-down aqueous fraction was resuspended in 200 µl of UPLC-grade water) was loaded per injection. UPLC separation of the lipid fraction was performed using a C8 reversed-phase column (100 μ m \times 2.1 μ m \times 1.7 μ m particles; Waters, Milford, MA, USA). Mobile phases were H₂O (ULC/MS; Biosolve) with 1% 1 mM NH₄Ac, 0.1% acetic acid (Buffer A) and acetonitrile: isopropanol (7:3, ULC/MS; Biosolve) containing 1% 1 mM NH₄Ac, 0.1% acetic acid (Buffer B). A 2 µl sample (of the dried-down organic fraction resuspended in 200 µl of acetonitrile: isopropanol (7:3)) was loaded per injection. Processing of chromatograms, peak detection, and integration were performed using REFINER MS 12.0

(Genedata, Basel, Switzerland). Processing of mass spectrometry data included removal of isotopic peaks and of chemical noise, retention time alignment and adduct detection. Metabolic features (m/z at a given retention time) were queried against an in-house reference compound library (allowing 10 ppm error and up to 0.2 min deviation from the retention time). Lipid annotation was based on a previously generated library of polar and lipophilic metabolites (Giavalisco *et al.*, 2011). See Dataset S1 for lipidomics mass spectrometry details.

Recombinant protein production

The START domain coding region of PDF2 was PCR amplified using gene-specific primers having ligation independent cloning (LIC) compatible extensions (Table S1). Gel-purified PCR product and SspI-digested pET-His6-MBP-TEV-LIC vector (Addgene, Watertown, MA, USA) were treated with T4 DNA polymerase with 25 mM dCTP and dGTP for 30 min at 22°C followed by heat inactivation. A 6 µl mixture of PCR product and vector was incubated at 22°C for 30 min, followed by addition of 1 µl 25 mM EDTA and E. coli transformation. Primers used to generate $pdf2^{L467P}$ via site-directed mutagenesis are listed in Table S1. E. coli BL21 Rosetta 2 (DE3) (Novagen, Madison, WI, USA) cells carrying pET-His6-MBP-TEV-PDF2 (START) and pdf2(START)^{L467P} were grown overnight in 5 ml LB with 40 μg ml⁻¹ kanamycin at 37°C. The next day, 0.5 l freshly prepared media was inoculated with 1 ml of culture and growth was continued at 28°C. At OD₆₀₀ 0.6, expression was induced with 0.5 mM IPTG (Sigma-Aldrich), followed by incubation at 16°C for 16 h. Cells were harvested by centrifugation at 4000 rcf, 10 min at 4°C, the pellet was frozen in liquid nitrogen and stored at -20° C for 1 h. The cells were resuspended in 20 ml of ice-cold lysis buffer containing 50 mM sodium phosphate pH 7.4, 500 mM NaCl, 1 mM imidazole, 0.5 mM TCEP, 1 mM PMSF (Sigma-Aldrich), 10% glycerol, 0.1% (w/v) lysozyme (AppliChem, Darmstadt, Germany) and cOmplete Protease Inhibitor Cocktail, EDTA free (Sigma-Aldrich). Bacterial slurry was sonicated in an ice-cold ultrasonic bath (RK 31; Bandelin) for 10 min, followed by centrifugation at 13 000 rcf for 10 min at 4°C. Supernatant was mixed with 2 ml of Ni-NTA agarose (Qiagen) on a rotary shaker for 1 h at 4°C. Ni-NTA beads with bound MBP-PDF2(START) protein were washed with 12 ml of ice-cold NaCl solutions. Protein was released from the beads using a step elution gradient (100-500 mM imidazole). Each step included 3 min incubations with 0.5 ml elution buffer containing 50 mM sodium phosphate pH 7.4, 500 mM NaCl, 0.5 mM TCEP, 1 mM PMSF, 10% glycerol, and increasing imidazole concentrations (100-500 mM). Concentration and purity of MBP-PDF2(START) in elution fractions was estimated by SDS-PAGE. Imidazole was removed and proteins were concentrated using Amicon Ultra 15 ml centrifugal filters with 10 kDa cutoff. Protein folding was assessed using nano differential scanning fluorimetry (nanoDSF). Aliquots of purified protein were stored at -20° C in 50 mM sodium phosphate buffer (pH 7.4) supplemented with 500 mM NaCl.

Liposome preparation

Lipids (Avanti Polar Lipids, Alabaster, AL, USA) were dissolved in chloroform. A total of 5 mg lipid for each liposome batch was dried in a glass tube under N₂ at 60°C. Residual chloroform was removed under vacuum overnight. Dried lipid cakes were rehydrated in 500 mM NaCl and 50 mM sodium phosphate (pH 7.4) at room temperature. Small unilamellar vesicles (SUVs) were formed by sonication using an ultrasonic bath (RK 31, Bandelin) for 15 min or by extrusion through two layers of polycarbonate membranes with 50 nm pore size (Nuclepore hydrophilic membrane; Whatman, Maidstone, UK) in a handheld extruder (Avanti Polar Lipids) or by sonication. Hydrodynamic radii of liposomes were determined by dynamic light scattering (DLS) to validate successful SUV formation.

Microscale thermophoresis

(MST) Microscale thermophoresis measurements performed using a Monolith NT.115 (NanoTemper, Munich, Germany). Capillaries were loaded into the instrument assets in 16-point ligand titrations. MBP-PDF2(START), MBP-PDF2 (START)^{L467P} were labeled in 50 mM sodium phosphate buffer (pH 7.4) supplemented with 500 mM NaCl using Monolith Protein Labeling kit RED-MALEIMIDE (NanoTemper) according to manufacturer's instructions. To remove the MBP tag, labeled proteins were incubated with Ni-NTA agarose (Oiagen) on a rotary shaker for 1 h at RT. Ni-NTA beads were washed with 50 mM sodium phosphate buffer (pH 7.4) supplemented with 500 mM NaCl before release with two rounds of TEV protease digestion, each with 30 U of TEV for 1 h at RT. Binding was performed in 50 mM sodium phosphate buffer (pH 7.4) supplemented with 500 mM NaCl using standard capillaries. MO. Affinity Analysis software (NanoTemper) was used to analyze binding affinities from changes in fluorescence. SDS-Test was performed according to the NanoTemper MST manual to exclude that observed changes in fluorescence were due to ligand induced changes in protein aggregation.

RNA extraction and quantitative real-time polymerase chain reaction

Plant samples of c. 50 mg were frozen in liquid nitrogen and stored at -80°C before RNA extraction with RNeasy Plant Mini Kit and on-column RNase-Free DNase Set (Qiagen). Total RNA (0.5 µg) was used as a template for cDNA synthesis with GoScript Reverse Transcriptase (Promega). Quantitative real-time polymerase chain reaction was performed using iTaq SYBR Green Supermix with the CFX96 Touch Real-Time PCR Detection System (Bio-Rad) with gene-specific primers (Table S1). Reactions contained 10 µl SYBR Green Supermix, 1 µl forward and reverse 10 µM primers, and 5 µl cDNA (diluted fivefold) in 20 µl. Standard curves were generated from 10-fold dilutions of amplicons for each primer pair. ACT7 served as the reference gene. Data represent at least 3–4 biological samples of seedling shoots with three technical replicates for each biological sample.

Lipid extraction from plant material

Plant tissues were transferred to hot isopropanol (70°C) with 0.01% BHT (butylated hydroxytoluene; Sigma) for 15 min followed by cooling to room temperature, and storage at -80°C before processing. Lipid extraction was done with chloroform: (isopropanol + methanol) : water (30 : 65 : 3.5). Samples were incubated overnight on a shakerat room temperature followed by solvent evaporation. Extracted lipids were transferred to 2 ml glass vials and dried under N_2 . Based on lipid dry weight and formula weight of c. 800 Da, lipids were eluted at 100 mM with chloroform. 100 μl of a 100 μM lipid mixture was dried under N_2 and stored at -80°C before analysis. Dried lipid fractions were resuspended in 200 μl UPLC-grade acetonitrile:isopropanol (7 : 3). A 2 μl sample was loaded per injection. LC/MS analysis was performed as described above. Raw intensities were normalized to the median of chromatogram intensity.

Imaging of plants and quantification of trichomes and roots

Seedlings, trichome phenotypes, and EYFP expression were imaged with a Leica M125 fluorescence stereo microscope fitted with a GFP2 filter set, and a Leica DFC295 digital camera with Leica Application Suite 4.1. Trichome quantification was performed as previously described (Schrick *et al.*, 2014). Root lengths were measured using IMAGEJ software analysis of seedling images from Bio-Rad Gel Doc XR+ Imaging System. Mature plants were imaged with a Canon PowerShot ELPH 350 HS digital camera.

In vitro transcription and translation and electrophoretic mobility shift assay (EMSA)

Wild-type (WT) and mutant PDF2 cDNAs were cloned from pENTR/SD/D-TOPO vectors (ABRC) into pIX-HALO (ABRC) using Gateway LR Clonase II Enzyme mix (Thermo Fisher Scientific). Halo fusion proteins were produced from 1.5 μg plasmid DNA in a 15 μl reaction using TNT SP6 High-Yield Wheat Germ Protein Expression System (Promega). Protein expression was confirmed by western blot with Anti-HaloTag monoclonal Ab (1:2000) (Promega) as the primary Ab and Goat Anti-Mouse IgG [HRP] (1:3000; GenScript A00160) as the secondary Ab. Cy3- or fluorescein (FAM)-labeled and unlabeled dsDNA probes were generated with oligonucleotides listed in Table S1. Annealing was performed with 25 µM oligonucleotides in 100 mM Tris-Cl (pH 7.5), 1 M NaCl, 10 mM EDTA at 95°C for 2 min, followed by 57°C for 5 min, 37°C for 90 min and 37°C for 2 min. EMSA reactions were prepared as previously described (Mukherjee et al., 2022). Binding reactions were performed with 200 nM (agarose gel) or 800 nM (or 9.2 µM for competition) of oligonucleotide probe (polyacrylamide gel). Electrophoresis of the protein-DNA complexes was at 4°C in a 0.6% agarose gel (1X TBE, pH 8.3) at 150 V for 1 h, or in a 7.5% polyacrylamide gel (456-1025, Bio-Rad) at 150 V for 4.5 h. The gels were analyzed with a Typhoon Trio Imager (GE Healthcare, Chicago, IL, USA) using high sensitivity

and the 532-nm green laser and 580-nm emission filter for Cy3 (600 PMT voltage) or the 488-nm blue laser and 520-nm emission filter for FAM (595 PMT voltage).

In vivo protein stability assay

At 5-6 d after germination on P+ or P- agar media, 20-30 seedlings per sample were transferred to liquid P+ or P- media and growth was continued for 16 h at 23°C under continuous light. Cycloheximide (Sigma-Aldrich) (400 µM final concentration) or DMSO was added at 0 h, and harvesting occurred at 0, 2, 5, 10 or 24 h. For proteasome inhibition experiments, cycloheximide was added together with MG132 (50 µM) (Sigma-Aldrich 474787) or DMSO control at 0 h. Seedling samples were frozen in liquid nitrogen and stored at -80° C before protein extraction. Tissue was homogenized in liquid nitrogen and hot SDS buffer (8 M urea, 2% SDS, 0.1 M DTT, 20% glycerol, 0.1 M Tris pH 6.8, 0.004% bromophenol blue) was added before SDS-PAGE and western blotting. Anti-HA (1:10 000; Pierce, Rockford, IL, USA) or Anti-GFP (1 : 2000; Roche) served as primary Abs, followed by Goat Anti-Mouse IgG [HRP] (1:3000; GenScript A00160) as the secondary. Proteins were detected with SuperSignal West Femto Maximum Sensitivity Substrate (Thermo Fisher Scientific) using an Azure 300 chemiluminescence imager (Azure Biosystems, Dublin, CA, USA), and blots were stained with Bio-Safe Coomassie Blue G-250 (Bio-Rad) to monitor protein loading. Band intensities were quantified with IMAGEJ.

Results

START domain of PDF2 recruits lysophospholipids in *Arabidopsis* cell cultures

To investigate binding partners of the START domain from PDF2 we used tandem affinity purification (TAP) adapted for parallel analysis of protein and metabolite interactors of the bait protein of choice (Luzarowski *et al.*, 2017, 2018) (Fig. 1a,b). We generated *Arabidopsis* cell lines expressing either full-length PDF2 or mutants lacking the START domain (pdf2^{ΔSTART}) under control of the constitutive CaMV 35S promoter, with a TAP tag fused to either the amino- or carboxyl end. Whole cell native protein lysates (referred to as input) from cultures expressing PDF2, pdf2^{ΔSTART} or empty vector were ultracentrifuged to deplete cellular membranes. TAP-tagged proteins were immunoisolated from soluble fractions and, following stringent washes, bait proteins together with interactors were released. The eluate was extracted yielding protein pellets, polar and nonpolar (lipid) metabolite fractions.

The presence of the bait protein was confirmed using mass spectrometry-based proteomics (Fig. 1c). We used an LC-MS lipidomics platform to identify lipids that co-purified with PDF2, and calculated the enrichment of specific lipids in the eluate in relation to the input. Comparison of PDF2 vs pdf2^{Δ START} cell lines (using input normalized data) identified 12 lipid species that were at least fourfold more abundant (*t*-test, P < 0.05; n = 6) in PDF2 vs pdf2^{Δ START} lines (Fig. 1d; Dataset S2). Of

the 12 differential lipid species, six were also at least fourfold more abundant (t-test, P < 0.05; n = 6) in PDF2 vs empty vector lines, constituting a list of high confidence lipid binders (Fig. 1d). The highest enrichment was for lysophosphatidylcholines (LysoPC 18:1 and LysoPC 18:2), with 14- and 22-fold enrichment over the empty vector and 7- and 12-fold enrichment over the pdf2^{Δ START} mutant (Fig. 1e). No differential lipid accumulation was found between the empty vector control and pdf2^{Δ START} lines (Dataset S2). Overall, the TAP experiments indicated that the START domain of PDF2 is associated with lipids, preferentially LysoPCs in *Arabidopsis* cell cultures.

START domain of PDF2 binds to LysoPCs in vitro

We next tested direct binding of PDF2 to LysoPCs in a reconstituted system. The *c.* 26 kDa START domain from PDF2 was produced in *E. coli* (Fig. S1a). Like mammalian STARD1/StAR (Sluchanko *et al.*, 2016), the PDF2 START domain, designated hereafter as PDF2(START), is highly insoluble when expressed in *E. coli*. To enhance solubility, the maltose binding protein (MBP) was fused to its amino terminus. The MBP tag was removed by TEV protease cleavage before binding analysis.

Alongside WT PDF2(START), we tested binding specificity using the mutant pdf2(START)^{L467P} having a missense mutation in the C-terminal α-helix that forms the lid of the binding pocket. L467 is a predicted lipid contact site (Roderick *et al.*, 2002), and the L467P mutation likely introduces a structural kink in the α-helix. Thus, this mutation could affect ligand binding by altering a ligand-binding site and/or by interfering with binding pocket closure. The C-terminal α-helix is conserved in START proteins from humans and plant HD-Zip IV TFs (Fig. 2a). Analogous L to P mutations in human StAR result in congenital lipoid adrenal hyperplasia, consistent with StAR loss-of-function (Bose *et al.*, 1996; Fluck *et al.*, 2005). Homology modeling (Roy *et al.*, 2010; Yang & Zhang, 2015) reveals structural similarity to START from PDF2 and GL2 (Fig. 2b). In GL2, the analogous L480P mutation leads to a loss-of-function phenotype in trichome cell differentiation (Fig. 2c,d) (Mukherjee *et al.*, 2022).

To examine binding of PDF(START) and pdf2(START)^{L467P} to lysophospholipids, we used microscale thermophoresis (MST) in conjunction with small unilamellar liposomes. Since LysoPC does not form liposomes on its own, we tested a 1:1 mixture of LysoPC and DOPC (36:2 PC; 1,2-dioleoyl-sn-glycero-3phosphocholine). We used liposomes carrying DOPC alone, and liposomes carrying another phospholipid, PG 34:2 (1-palmitoyl-2-linoleoyl-sn-glycero-3-phosphoglycerol) as controls (Figs 2e, S1b-d). The presence of LysoPC 18:1 favored interaction with WT PDF2(START) over the mutant. Specifically, the binding affinity to DOPC/LysoPC 18:1 liposomes was c. 12-fold greater for PDF2 (START) ($K_d = 17 \mu M$) in comparison to pdf2 $(START)^{L467P}$ ($K_d = 200 \mu M$) (Fig. 2e). By contrast, the binding data show that WT PDF(START) and mutant pdf2 (START)^{L467P} bind DOPC and PG 34:2 liposomes with comparable affinities. These in vitro binding data indicate that PDF2 associates with and directly binds LysoPCs through its START domain, consistent with our TAP results (Fig. 1).

xaded from https://nph.onlinelibrary.wiley.com/doi/10.1111/nph.19917 by Kathrin Schrick

- Kansas State University, Wiley Online Library on [02/07/2024]. See the Terms

) on Wiley Online Library for rules of use; OA articles are governed by the applicable Crea

We investigated a possible regulatory connection between PDF2 and phospholipids. Previously reported genome-wide DNA

affinity purification sequencing (DAP-seq) peak data (O'Malley et al., 2016) for PDF2 revealed the palindrome GAATATTC as the main DNA-binding motif (Fig. 3a). This octamer displays consensus to the previously identified P1BS element (GNATATNC) (Rubio et al., 2001). Under Pi limitation, P1BS is the

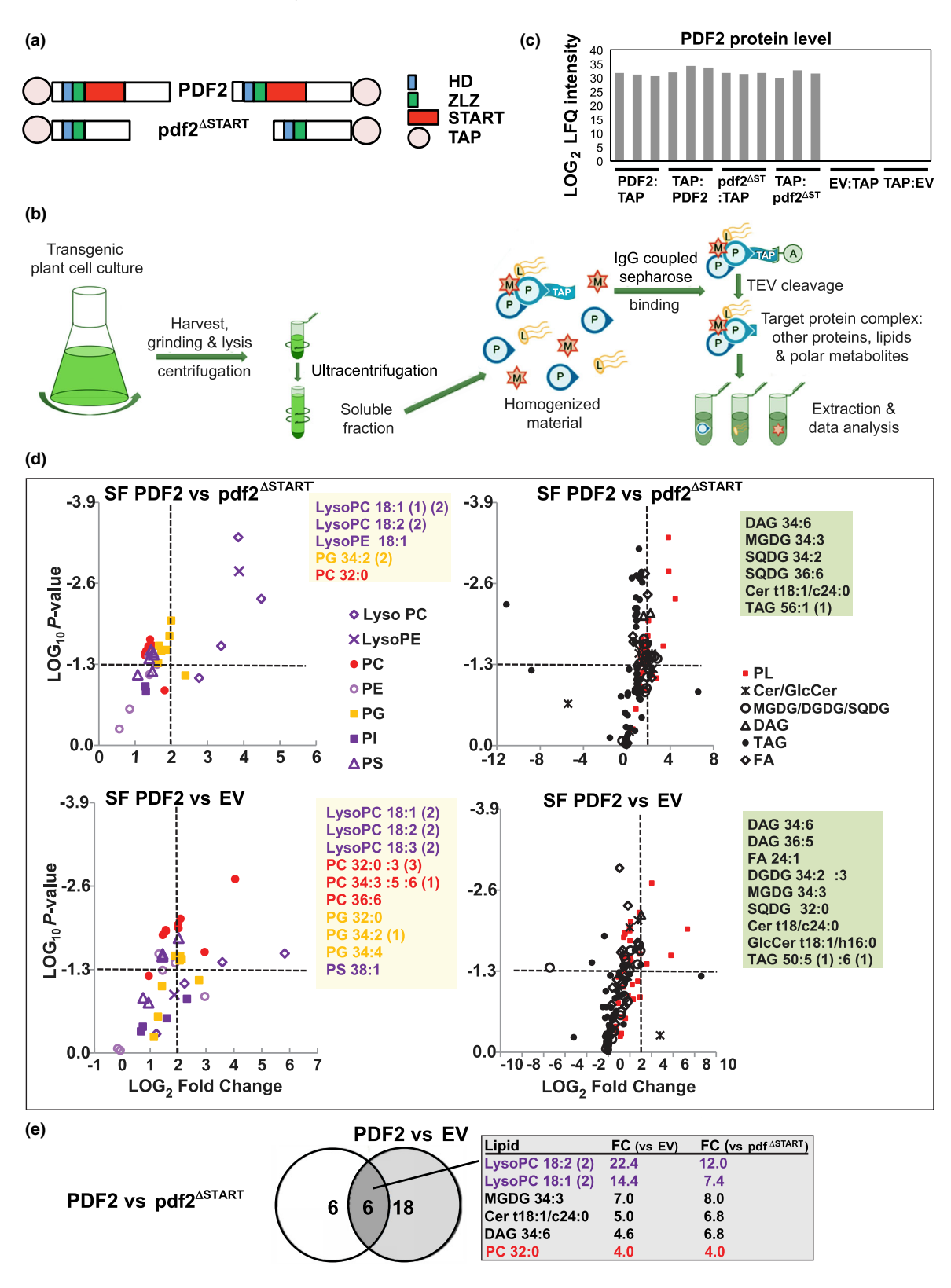


Fig. 1 PDF2 START binds lysophosphatidylcholine (LysoPC) in *Arabidopsis* cell cultures. (a) PDF2 and pdf2^{ΔSTART} proteins used for tandem affinity purification (TAP) experiments. HD, Homeodomain; ZLZ, zipper loop zipper, a plant-specific leucine zipper; START domain. (b) Schematic of TAP protocol with *Arabidopsis thaliana* cell cultures. (c) PDF2 protein quantification from eluates obtained from TAP. Mass spectrometry-based proteomics revealed similar label-free quantification (LFQ) intensities for cell lines expressing full-length PDF2 and mutant pdf2^{ΔSTART}. No signal was detected for empty vector (EV) lines. (d) Lipidomic analysis shows that the START domain of PDF2 recruits lysophosphatidylcholine (LysoPC). Lipids were extracted from TAP eluates from PDF2, pdf2^{ΔSTART} and EV lines and analyzed by LC/MS. Volcano plots depict log_2 -fold changes (FC) between PDF2 and either pdf2^{ΔSTART} or EV on x axis vs significance (*P*-values, unpaired *t*-test) on *y* axis for means of six replicate cell cultures. Horizontal dotted line indicates P = 0.05. Vertical dotted line marks a ratio of 4. SF, soluble fraction. Volcano plots of phospholipid (PL) changes in phosphatidylcholine (PC), phosphatidylethanolamine (PE), phosphatidylglycerol (PG), phosphatidylinositol (PI), and phosphatidylserine (PS) (left). Volcano plots of lipid profiles represent values for PL, ceramides (Cer), glucosylceramides (GlcCer), digalactosyldiacylglycerols (DGDG), monogalactosyldiacylglycerols (MGDG), sulfoquinovosyl diacylglycerols (SQDG), diacylglycerols (DAG), triacylglycerols (TAG), and fatty acids (FA) (right). Lipid interactors are shown in boxes (4-FC, *t*-test, *P* < 0.05). The colored boxes indicate which lipids are enriched in wild-type PDF2 in comparison to either mutant pdf2^{ΔSTART} or the EV control. For each lipid metabolite, the first and second numbers separated by a colon indicate the number of carbons and double bonds in fatty acid chains, respectively. The parentheses next to each lipid species indicate differen

binding site of PHOSPHATE STARVATION RESPONSE 1 (PHR1), which positively regulates phospholipid remodeling and other aspects of the Pi starvation response (Pant *et al.*, 2015).

To validate that PDF2 binds the P1BS palindrome, we performed electrophoretic mobility shift assays (EMSA) with *in vitro* translated proteins and a fluorescently labeled oligonucleotide containing GAATATTC. The WT PDF2 and the mutant pdf2^{ΔST} proteins caused a shift in mobility of the fluorescent probe, in contrast to missense mutant pdf2^{K107E} in which a conserved arginine in the HD DNA-binding domain is replaced with glutamic acid (Fig. 3b,c). Our EMSA competition experiments indicated binding with an unlabeled oligonucleotide containing the WT but not a mutant P1BS element (Fig. 3c). The results additionally show that, while the HD is required for binding to the P1BS palindrome, the START domain of PDF2 is dispensable for DNA binding, as previously reported for PDF2 binding to the L1 box (Mukherjee *et al.*, 2022).

PDF2 transcriptional targets include phospholipid- and Pi starvation-related genes

The binding of PDF2 to the P1BS palindrome may affect the gene expression of nearby genes, and such genes are candidates to be transcriptional targets of PDF2. We mined the available PDF2 DAP-seq data (O'Malley *et al.*, 2016) for candidate transcriptional targets using the PANTHER (Mi *et al.*, 2019) overrepresentation test. The top gene ontology (GO) terms were 'phospholipid catabolic process' and 'cellular response to phosphate starvation' and these displayed enrichment of *c.* 9.8-fold and *c.* 6.3-fold, respectively (Fig. 3d; Dataset S3).

We scanned the genomic regions from candidate gene targets for overlap between DAP-seq peaks and P1BS palindromes (Figs 3e, S2a). Matches of 100% were found in the promoters or 5 '-UTR regions of several Pi starvation-induced genes, including those encoding a glycerophosphodiester phosphodiesterase (GDPD1) (Cheng et al., 2011), an SPX domain-containing nuclear protein (SPXI) (Puga et al., 2014), a nonspecific phospholipase C (NPC4) (Nakamura et al., 2005) (Fig. 3e), and other phospholipid- or Pi starvation-related candidates (Fig. S2a). These observations suggested that PDF2 transcriptionally

regulates genes that are involved in phospholipid metabolism and/or Pi sensing.

PDF2 is a transcriptional regulator of phospholipid- and Pi starvation-related genes

To test whether PDF2 controls the mRNA expression of the candidate transcriptional targets, we applied reverse transcription quantitative polymerase chain reaction in conjunction with mutant analysis. Since *PDF2* is expressed in the epidermis and the DAP-seq experiment utilized genomic DNA from young leaves (O'Malley *et al.*, 2016), we extracted mRNA from seedling shoots. This material contains epidermis as well as other tissues that do not express *PDF2*. Therefore, we considered small differences from WT, if statistically significant, to be indicative of altered gene expression in mutants.

For this analysis we utilized previously characterized T-DNA insertion mutants of PDF2 and other HD-Zip IV genes ATML1 and GL2 (Fig. 3f). Our quantitative real-time polymerase chain reaction analysis revealed differences in PDF2 mRNA levels for each of the pdf2 alleles (Fig. 3g). The null mutant allele, pdf2-4, in which the T-DNA insertion occurs before the HD (Kamata et al., 2013b), exhibited a c. threefold increase in mRNA. By contrast, the pdf2-1 and pdf2-2 alleles, in which the T-DNA insertion disrupts the START domain, result in lower levels of the transcript (Fig. 3g). The pdf2-1 partial function mutant showed approximately WT levels of PDF2 transcript, as previously reported (Kamata et al., 2013a). By contrast, the pdf2-2 allele resulted in c. twofold lower levels of PDF2 expression (Fig. 3g). Strikingly, the EYFP:pdf2^{AST} transgenic line in which the START domain is deleted exhibited a similar reduction in mRNA levels as the pdf2-2 allele (Fig. 3h). The difference in endogenous PDF2 mRNA expression for WT EYFP:PDF2 vs mutant EYFP:pdf2^{AST} (Fig. 3h) cannot be attributed to differences in transgene expression because the transgenes exhibit similar levels of mRNA (Fig. 3i).

We performed quantitative real-time polymerase chain reaction with several candidate transcriptional targets from the DAP-seq data (Figs 3e, S2b). The quantitative real-time polymerase chain reaction data show that, in comparison to WT, the

14698137, 0, Downloaded from https://nph.onlinelibrary.wiley.com/doi/10.1111/nph.19917 by Kathrin Schrick - Kansas State University , Wiley Online Library on [02/07/2024]. See the Terms

on Wiley Online Library for rules of use; OA articles are governed by the applicable Creative Commons

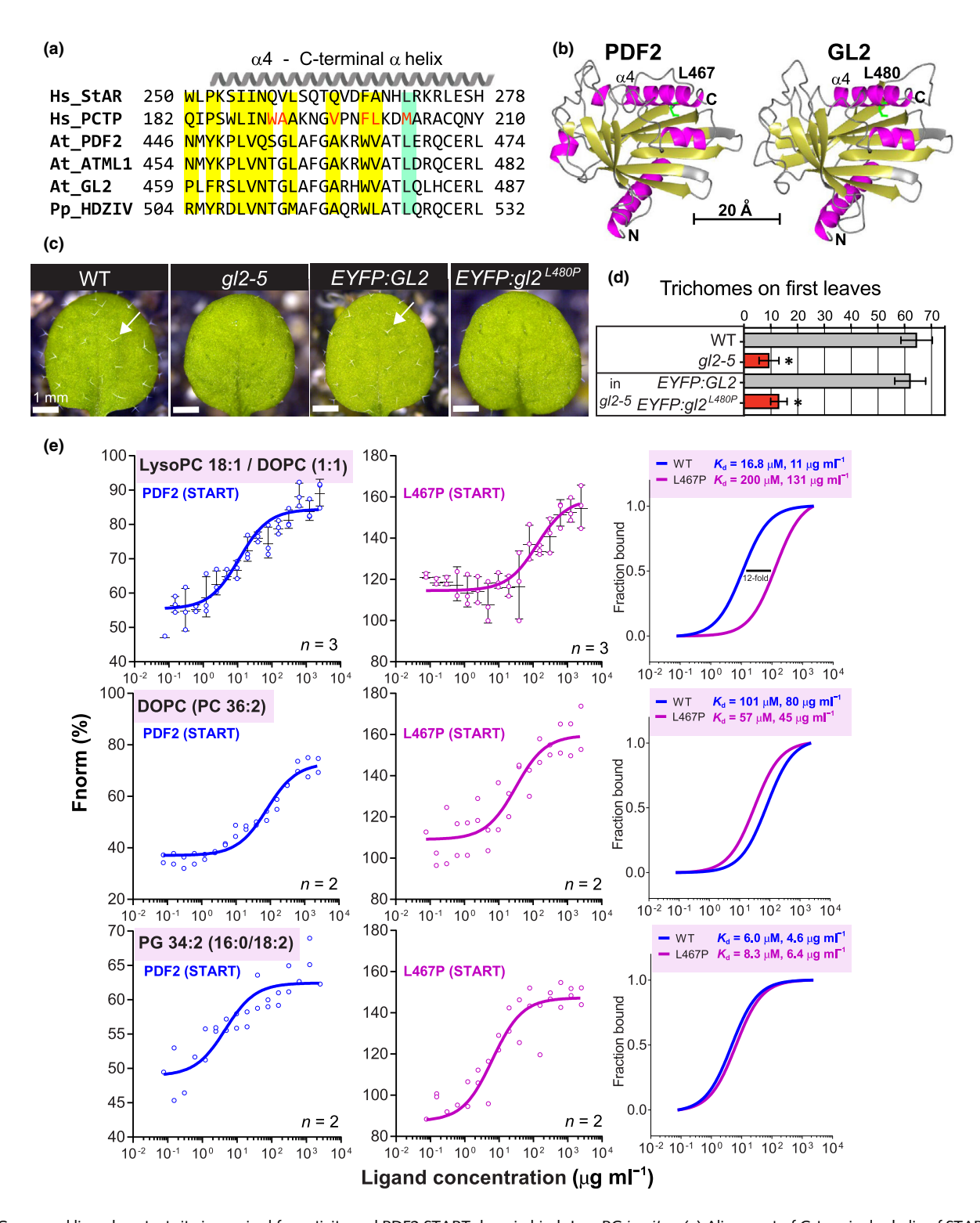


Fig. 2 Conserved ligand contact site is required for activity and PDF2 START domain binds LysoPC *in vitro*. (a) Alignment of C-terminal α-helix of START from human (Hs) StAR and PCTP, and HD-Zip IV TFs from *Arabidopsis thaliana* (At) and *Physcomitrium patens* (Pp). Conserved amino acids (bold, yellow); conserved Leu/Met (green). Ligand contact sites as determined from PCTP-PC co-crystal (Roderick *et al.*, 2002) (red). (b) Structural homology models of PDF2 and GL2 START domains generated in I-TASSER (Roy *et al.*, 2010; Yang & Zhang, 2015) reveal conserved Leu (green) in C-terminal α-helix. (c) First leaves expressing proGL2:EYFP:GL2 vs $proGL2:EYFP:gl2^{L480P}$ in gl2-5 background in comparison to wild-type (WT) and gl2-5. Normal trichomes on leaves of WT (arrows) but not mutant gl2. Bar, 1 mm. (d) Quantification of leaf trichomes: $gl2^{L480P}$ mutants exhibit trichome defects similar to gl2-5. Error bars indicate SD for $n \ge 20$ plants. Significant differences for $gl2^{L480P}$ vs WT (unpaired t-test): *, P < 1.0E-10. (e) PDF2 START domain binds to LysoPC 18:1 *in vitro*. Binding of purified WT PDF2(START) or mutant pdf2(START)^{L467P} to liposomes prepared using indicated lipids and lipid mixtures and measured by microscale thermophoresis (MST). Mean \pm SD is shown for n = 3 independent titrations, and individual data points are shown for n = 2-3 independent titrations. Dose response curves were used to calculate binding affinities expressed as dissociation constants K_d . See also Supporting Information Fig. S1.

phospholipid catabolic gene *GDPD1* was upregulated in *pdf2* mutants, but not in *atml1* or *gl2* mutants (Fig. 3j). *SPX1*, which encodes a transcriptional regulator associated with the Pi starvation response (Puga *et al.*, 2014), showed remarkably similar regulation (Fig. 3j). The *NPC4* gene also showed upregulation in *pdf2-1* mutants, but the expression profiles were not as consistent. We observed inconsistencies in gene regulation of other predicted transcriptional targets, some of which had DAP-seq peaks in their promoter or 5 '-UTR (Fig. S2a). For these gene target candidates, complex regulatory mechanisms may only partially or transiently involve PDF2 function.

To examine the expression of the selected candidate transcriptional target genes under Pi sufficiency and starvation, we tested pdf2-4 null mutants alongside WT and pdf2-1 mutants. Consistent with previous studies (Nakamura et al., 2005; Cheng et al., 2011; Puga et al., 2014), WT showed upregulation of GDPD1, SPX1 and NPC4 under Pi limitation (Fig. 3k). The pdf2 mutants exhibited further upregulation of these three genes under PI limitation (Fig. 3k), suggesting that PDF2 plays a role in fine-tuning gene expression in response to Pi availability. The robust upregulation of GDPD1 in all of the pdf2 mutant alleles that we tested is consistent with a role for PDF2 in transcriptional repression of that gene. Overall, the data indicate that PDF2 activity is required for maintaining normal transcript levels of GDPD1 and a few other phospholipid- and Pi response-related genes (SPX1, NPC4) at the seedling stage and Pi conditions that we tested.

Repressor activity of PDF2 requires the START domain

We asked whether ectopic expression of PDF2 can drive repression of the selected transcriptional targets by comparing transgenic lines expressing EYFP:PDF2 with the mutant EYFP: pdf2^{AST} which lacks the START domain (Fig. 3l). The WT EYFP:PDF2 expression, but not EYFP:pdf2^{AST}, resulted in downregulation of GDPD1, SPX1 and NPC4 (Fig. 31). This expression pattern was not observed under Pi limitation, likely due to low levels of mRNA expression of the EYFP-tagged transgenes relative to the endogenous PDF2 gene (Fig. 3i,j). Other candidate gene targets failed to show consistent PDF2-dependent regulation in our experiments (Fig. S2). Nonetheless, our PDF2 ectopic expression studies together with our mutant analysis (Fig. 3j,k) provides evidence that PDF2 acts a transcriptional repressor of at least three transcriptional target genes that have functions related to phosphate response (GDPD1, SPX1, and NPC4). Moreover, comparison of the WT EYFP:PDF2 and mutant EYFP:pdf2^{\Delta ST} transgenic lines indicates that the START domain is required for transcriptional repression.

Lipidomic profiling of mutants reveals defects in phospholipid homeostasis

We next focused on the link between PDF2 and phospholipid metabolism. Gene expression changes in the phospholipid catabolic genes *GDPD1* and *NPC4* are expected to result in altered phospholipid profiles and abnormal membrane lipid remodeling.

We performed a lipidomic analysis from the same shoot tissues as those used for quantitative real-time polymerase chain reaction. Our LC-MS platform targeted > 240 lipid species including phospholipids (LysoPC, PC, PE, PG, PI, PS), sphingolipids (ceramides (Cer) and glucosylceramides (GlcCer)), glycolipids (DGDG, MGDG, SQDG), diacyl- and triacylglycerols (DAG, TAG), and fatty acids (FA). Representative lipids from each major class were quantified in WT and mutants for PDF2, ATML1 and GL2. (Dataset S4; Figs S3, S4). Double mutants for atml1-1 and pdf2-1 display morphological defects at the seedling stage (Fig. S4a) (Abe et al., 2003), and we detected significant differences from WT in > 100 lipid species (Fig. S3b; Dataset S4; Table S2). Notably, the phospholipids LysoPC, PE, PI, and PS were generally increased in atml1;pdf2. Other lipids that showed increases included DAGs, TAGs, FA, and Cer, while GlcCer, DGDG, MGDG, and SQDG were decreased (Dataset S4; Fig. S3c). Since the atml1;pdf2 double mutants display developmental defects (Abe et al., 2003), the associated lipid changes may be attributed to their abnormal physiology. The other HD-Zip mutants, which display normal growth patterns, showed phospholipid defects to a lesser extent. For example, the pdf2-1 single mutants exhibited increases in several PC and PS lipids. Alterations in DAG, TAG, galactolipids and FA were additionally observed, as expected from membrane lipid remodeling (Dataset \$4; Fig. \$4).

START domain is critical for phospholipid and FA homeostasis

In a second lipidomics experiment we monitored lipid composition under Pi sufficiency and limitation for pdf2, atml1 and gl2 single mutants in comparison to WT (Dataset S5; Figs 4a, S5, S6). To address the role of the START domain in lipid homeostasis, we included transgenic lines that were either WT (PDF2 and GL2) or mutant for the START domain (pdf2^{AST} and gl2^{L480P}). These transgenes were expressed as EYFP-tagged proteins in the gl2-5 background under the GL2 promoter, which drives expression in specialized epidermal cell types including trichomes (Khosla et al., 2014). We included three pdf2 alleles (pdf2-1, pdf2-2 and pdf2-4). Based on the position of their T-DNA insertion (Fig. 3f), pdf2-4 represents a null allele (Kamata et al., 2013b), while the pdf2-1 and pdf2-2 alleles are both expected to affect the function of the START domain. Likewise, atml1-3 represents a null allele (Fig. 3f), whereas atml1-4 affects START but not the HD.

Pi limitation resulted in lower levels of phospholipids in WT, as previously reported (Li *et al.*, 2006), and we observed this trend in all the lines (Dataset S5; Figs 4a, S6). In comparison to WT, the *pdf2-2* seedlings exhibited a notably altered phospholipid profile: LysoPCs were significantly increased, and others (PC, PG, PS) were increased or decreased under Pi sufficiency, whereas >30 phospholipids (LysoPC, PC, PE, PG, PS) exhibited enhanced accumulations FC \geq 2 under Pi limitation (Fig. 4a). The *pdf2-1* mutants also exhibited altered levels of several PCs, as well as other abnormal lipid accumulations, especially TAGs and FAs, similar to *pdf2-2*, and these defects were more pronounced

4698137, 0, Downloaded from https://nph.onlinelibrary.wiley.com/doi/10.1111/nph.19917 by Kathrin Schrick

- Kansas State University, Wiley Online Library on [02/07/2024]. See the Terms

) on Wiley Online Library for rules of use; OA articles are governed by the applicable Creat

under Pi limitation (Figs 4a–d, S4, S6; Tables S3, S4). The lipid defects in *pdf2-2* were more severe than those in the *pdf2-1* mutants, possibly due to enhanced stability of the corresponding truncated protein resulting in more DNA-binding activity from *pdf2-2* allele.

We compared lipid profiles of seedlings expressing WT EYFP:PDF2 to the $EYFP:pdf2^{AST}$ mutant. Strikingly, $pdf2^{AST}$ exhibited FC ≥ 2 increases in LysoPCs (16:0, 18:2, 18:3) and several other phospholipids under Pi limitation (Figs 4c, S6; Table S5). Similarly, when we compared WT EYFP:GL2 to

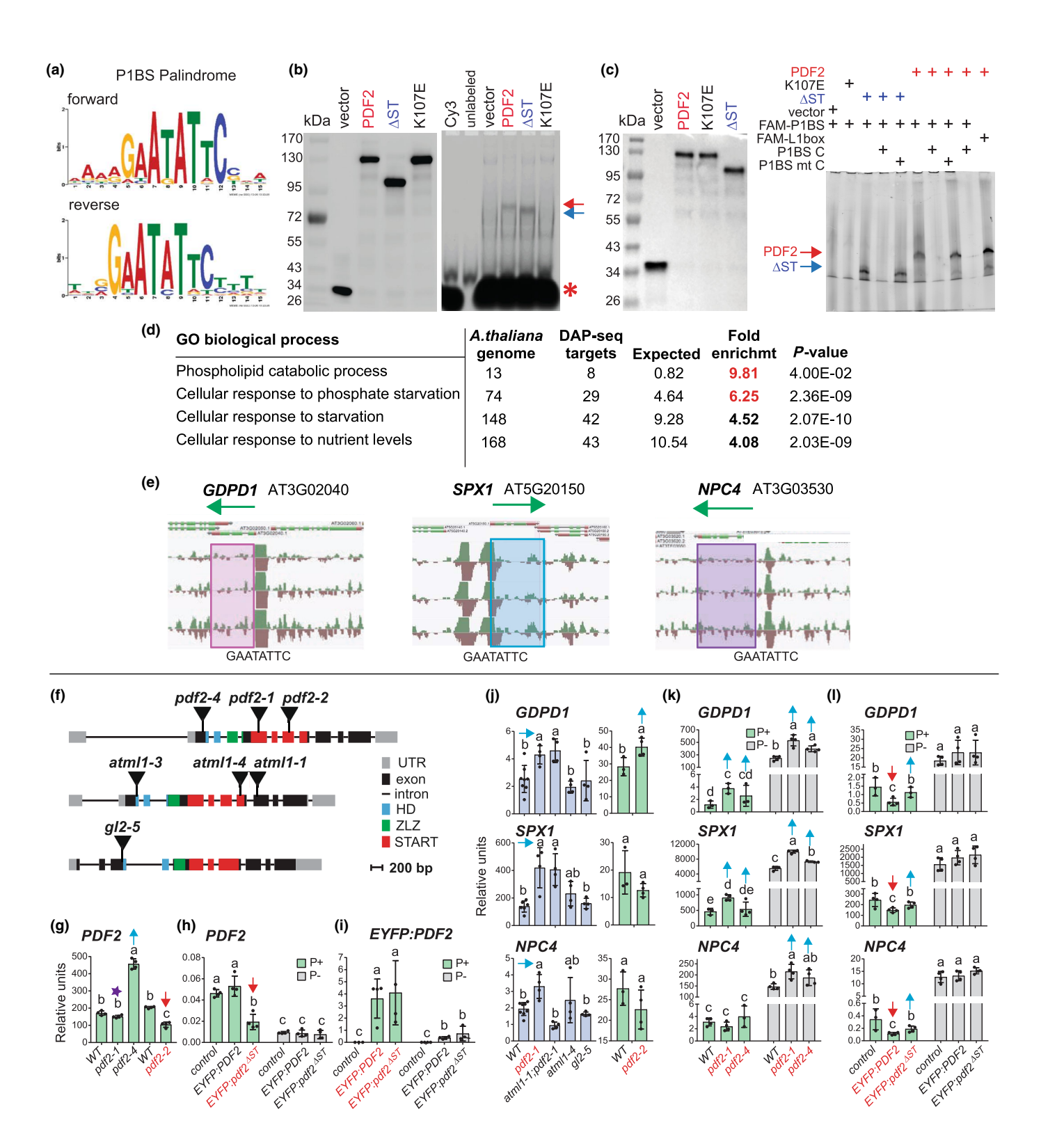


Fig. 3 PDF2 binds a Pi response element and acts as transcriptional regulator of phospholipid- and Pi starvation-related genes. (a) Palindromic octamer motif from DAP-seq data (O'Malley et al., 2016) for PDF2 exhibit consensus with P1BS (GNATATNC). (b, c) EMSAs show band shift for Halo:PDF2 and pdf2^{AST} (arrows) but not for Halo from vector control nor for HD mutant pdf2^{K107E} (right). Western blot with anti-Halo Ab detects Halo-tagged proteins used in EMSA (left). (b) EMSA with agarose gel and Cy3-labeled probe (asterisk) containing GAATATTC. Representative gel from three independent experiments. (c) EMSA with polyacrylamide gel and FAM-labeled probe containing GAATATTC in absence or presence of 11.5-fold excess of unlabeled wild-type (WT) or mutant competitor oligonucleotide. Only the unlabeled WT competitor (C) probe competes for binding with the labeled probe. Binding of PDF2 to the L1 box is included for comparison. Representative gel from two independent experiments. (d) Statistical overrepresentation of phospholipid- and Pi starvation-related genes from analysis of DAP-seq target genes of PDF2. See Supporting Information Dataset S3(b). (e) Putative transcriptional targets of PDF2 show DAP-seq peaks that map to GAATATTC on forward (green) and reverse (brown) strands. Green arrows indicate length and direction of transcript. Shaded boxes mark the position of the transcript and are colored according to target gene classification: phospholipid enzyme GDPD (pink), SPX transcriptional regulator (blue), phospholipid enzyme NPC (purple). See Fig. S2(a,b). (f) Genomic DNA map positions of T-DNA insertions for PDF2, ATML1 and GL2. T-DNA insertions are shown relative to the gene segments encoding the homeodomain (HD), zipper loop zipper (ZLZ), and START domain. (g) Quantitative real-time polymerase chain reaction with cDNA from 14-d-old seedling Arabidopsis thaliana shoots shows that PDF2 mRNA is upregulated in pdf2-4 and downregulated in pdf2-2 (arrows). (h, i) Quantitative real-time polymerase chain reaction with cDNA from 14d-old seedling shoots under Pi sufficiency (P+) or limitation (P-). (h) Endogenous PDF2 mRNA is downregulated by ectopic expression of EYFP: $pdf2^{\Delta ST}$ under Pi sufficiency (arrow). (i) The EYFP:PDF2 and EYFP:pdf2^{AST} lines display similar mRNA levels of the EYFP transgene. (j) Quantitative real-time polymerase chain reaction with cDNA from 12 d-old (WT, pdf2-1, atml1-1;pdf2-1, atml1-4, gl2-5) or 15 d-old (WT, pdf2-2) seedling shoots. PDF2 is required for normal mRNA expression of GDPD1, SPX1, and NPC4. (k, l) Quantitative real-time polymerase chain reaction with cDNA from 14-d-old seedling shoots under Pi sufficiency (P+) or limitation (P-). (k) PDF2 is required for normal gene expression of GDPD1 and SPX1 under both Pi sufficiency and limitation, and PDF2 is required for normal NPC4 expression under Pi limitation. (I) Ectopic expression of WT EYFP:PDF2 but not START mutant EYFP: $pdf2^{AST}$ results in downregulation of GDPD1, SPX1, and NPC4 under Pi sufficiency. (g-l) Data represent means of at least n=3-4 biological replicates normalized to reference gene ACT7. Error bars indicate SD. Arrows indicate transcriptional upregulation (blue) in pdf2 mutants and downregulation (red) by PDF2 ectopic expression in (j-l). Significant differences between genotypes determined by one-way ANOVA, Tukey's test, and indicated by letters: P < 0.05. See also Fig. S2(c-e).

START domain mutant $EYFP:gl2^{L480P}$ we also noted lipid changes that varied with Pi status: LysoPC 18:2 and several FAs were elevated FC ≥ 2 in $gl2^{L480P}$ under Pi limitation (Fig. S6; Dataset S5). We compared lipid changes in pdf2-2 and $pdf2^{\Delta ST}$ which both affect START domain function (but not HD DNA binding) and both exhibit reduced levels of endogenous PDF transcript (Fig. 3h,i). Under Pi limitation, pdf2-2 and $pdf2^{\Delta ST}$ shared numerous phospholipid increases in comparison to controls (Fig. 4c; Tables S4, S5). We also observed increases in numerous FA species in both START domain mutants (Fig. 4d). Overall, the results suggest the strongest imbalances in phospholipid and FA levels in the pdf2 START domain mutants, notably under Pi starvation.

PDF2 drives elongation growth in the root that is dependent on START and HD domain activity

To examine the role of HD-Zip IV genes in regulating growth according to Pi status, we assayed WT seedlings alongside *pdf2*, *atml1* and *gl2* mutants for vertical root elongation in Pi sufficient and limiting media (Fig. 5a). For this experiment we included the *pdf2-4* null mutant in comparison to the *pdf2-2* START mutant that had resulted in a severe lipid phenotype. Both the *pdf2-2* and *pdf2-4* mutants exhibited decreased elongation growth under Pi sufficiency, while the *atml1-3* and *gl2-5* mutants appeared indistinguishable from WT (Fig. 5b). Under Pi limitation, the *pdf2-2* mutant had a more pronounced defect in root elongation and the *pdf2-4* mutant showed a slight decrease (Fig. 5b). By contrast, root elongation appeared mildly increased for the *atml1-3* and *gl2-5* mutants under Pi limitation.

We next examined seedlings expressing *EYFP:PDF2* under the epidermal specific *GL2* promoter in the *gl2-5* background. The *GL2* promoter drives expression in trichomes and in nonroot hair

cells (Khosla et al., 2014), which undergo extensive elongation in the seedling. Expression of WT EYFP:PDF2, but not HD mutant $EYFP:pdf2^{K107E}$ or START mutant $EYFP:pdf2^{\Delta ST}$, partially rescued the trichome defect of gl2-5 (Fig. 5c,d). To further test whether PDF2 is critical for elongation growth we measured root lengths in EYFP:PDF2 vs EYFP: $pdf2^{\Delta ST}$ seedlings (Fig. 5e, f). The data indicate that ectopic expression of WT PDF2 under both Pi sufficiency and limitation results in increased elongation, whereas elongation in $pdf2^{K107E}$ or $pdf2^{\Delta ST}$ was indistinguishable from the control. At later stages, we observed growth defects and aberrant leaf morphologies in the PDF2 expressing lines, but not in pdf2K107E or pdf2\DeltaST lines (Fig. S7). EYFP-tagged PDF2 protein exhibited nuclear localization under both Pi sufficiency and limitation (Fig. 5g), and mutant pdf2 proteins were similarly expressed in nuclei (Fig. 5h). The data indicate that ectopic epidermal PDF2 expression drives elongation growth in the primary root, and the observed growth phenotype is dependent on both the HD and START domains. Our results corroborate our finding that both the pdf2-4 null mutant (which abolishes HD function) and the pdf2-2 mutant (which abolishes START function) are defective in elongation growth.

START domain mutation L480P affects elongation growth and repression of target gene $PLD\zeta 1$ by GL2

We further tested whether the START domain is required to control elongation growth by comparing *gl2-5* seedlings stably expressing *proGL2:EYFP:GL2* or *proGL2:EYFP:gl2^{L480P}*. The START domain mutation L480P leads to trichome defects (Figs 2d, 6a) (Mukherjee *et al.*, 2022). Additionally, the *gl2^{L480P}* seedlings displayed slightly decreased root elongation under Pi sufficiency, and increased elongation in comparison to WT under Pi limitation (Fig. 6b). Our quantitative real-time polymerase

.4698137, 0, Downloaded from https://nph.onlinelibrary.wiley.com/doi/10.1111/nph.19917 by Kathrin Schrick

- Kansas State University, Wiley Online Library on [02/07/2024]. See the Terms

) on Wiley Online Library for rules of use; OA articles are governed by the applicable Creative Commons License

 $EYFP:gl2^{L480P}$ transgenes were expressed (Fig. 6c), arguing against the possibility that the mutant phenotype is due to the lack of mRNA expression.

pdf2-4-atml1-3-atml1-4-gl2-5-WT-pdf2-1-pdf2-2-

gl2-5atml1-3

Ņ pdf2-1 df2ΔST. odf2 AST

PDF2

atml1-3 } atml1-4 } atml1-4 } a

pdf2-2-pdf2-4-

GL2-gl2L480P-

GL2-gl2 L480P-GL2-gl2 L480P

previously identified phospholipase target gene of GL2, namely $PLD\zeta I$ (Ohashi *et al.*, 2003), whereas the mutant $EYFP:gl2^{L480P}$ failed to show this transcriptional repression (Fig. 6d). Consistent



(b)

Signal intensity

3000-

2000 1000

Fig. 4 Lipidomic profiling reveals elevated phospholipid and FA levels in pdf2 START mutants under Pi limitation. (a, b) Lipids were extracted from 14-d-old seedling Arabidopsis thaliana shoots from wild-type (WT), pdf2, atml1, and gl2 mutants as well as EYFP:PDF2, $EYFP:pdf2^{AST}$, EYFP:GL2 and $EYFP:gl2^{L480P}$ transgenic lines, followed by LC-MS. Data represent 4–5 biological replicates for each genotype under Pi sufficiency (P+) or limitation (P-). Values for biological replicates are given in Supporting Information Dataset S5. Signal intensities are indicated for means of lipid classes. Error bars indicate SD. Significant differences between > 3 genotypes are marked by letters (one-way ANOVA, Tukey's test) and between 2 genotypes by unpaired t-test: *, P < 0.05. Arrows indicate elevated levels of phospholipids (PL) (a) or fatty acids (FA) (b) in both pdf2-2 and $pdf2^{AST}$ mutants. Most significant differences are seen under Pi limitation. Fig. S5 shows data for other lipids. (c and d) Heat maps of (c) selected PL and (d) all FA levels under Pi limitation in WT and pdf2 mutants in comparison to EYFP:PDF2 and $EYFP:pdf2^{\Delta ST}$. Only PL species with significant increases in $pdf2^{AST}$ after FDR analysis are shown in the PL heat map (Table S4). Parentheses next to lipid species indicate alternative combinations of fatty acid chains corresponding to nomenclature for numbers of carbons and double bonds. Minimum and maximum values were normalized to 0.0 and < 1.0, respectively, for visualization purposes. See Fig. S6 and Dataset S5.

with our finding that the *EYFP:GL2* and *EYFP:gl2^{L480P}* transgenes are expressed at the mRNA level (Fig. 6c), both WT and mutant EYFP-tagged proteins were visible and both exhibited nuclear localization (Fig. 6e), despite loss of transcriptional repressor activity of the gl2^{L480P} mutant protein. Therefore, the differential root elongation phenotype of mutant $gl2^{L480P}$ vs WT GL2 as well as our quantitative real-time polymerase chain reaction analysis with the phospholipase target gene $PLD\zeta 1$ suggests that a functional START domain is critical for normal elongation growth and target gene repression of $PLD\zeta 1$ in response to Pi availability.

PDF2 and GL2 exhibit reduced protein stability under Pi limitation, and protein instability is enhanced in START mutants

Time-course microarray profiles of Arabidopsis thaliana seedlings previously indicated that PDF2, ATML1 and GL2 transcripts are not significantly up- or downregulated in the initial response to Pi starvation (Lin et al., 2011). However, our quantitative realtime polymerase chain reaction data show that prolonged Pi limitation results in downregulation of both PDF2 and GL2 mRNA in seedlings (Figs 3i, 6c), possibly due to feedback mechanisms affecting TF function. We next examined whether the PDF2 and GL2 proteins are posttranslationally regulated by Pi availability. Cycloheximide assays with seedlings expressing hemagglutinin (HA)- or EYFP-tagged TFs were performed to track the stability of the proteins in the presence or absence of Pi. We noted that EYFP:PDF2 displayed increased stability in comparison to HA: PDF2 (Fig. 7a), similar to the higher stability of EYFP:GL2 in comparison to HA:GL2 (Fig. 7b) that was previously reported (Subedi & Schrick, 2022). The reason for the increased stability due to the presence of the EYFP tag is not known, but it was speculated that this tag may interfere with degradation by some unknown mechanism (Subedi & Schrick, 2022).

Regardless of the epitope tag, both the PDF2 and GL2 proteins exhibited increased turnover under Pi limitation (Figs 7a–c, S8). In comparison to WT EYFP:PDF2, the mutant EYFP: pdf2^{ΔST} protein tended to be less stable under Pi sufficiency, and this instability was enhanced to under Pi limitation (Fig. 7c). Similarly, in comparison to WT EYFP:GL2, which is relatively stable at 24 h under Pi sufficiency, the EYFP:gl2^{L480P} mutant protein exhibited a decrease in stability and half-life of *c*. 10 h (Figs 7d, S8). The half-life of EYFP:gl2^{L480P} was further reduced

to *c*. 2 h under Pi limitation (Fig. 7d), indicating that START is critical for protein stability under both conditions. Coincubation of seedlings under Pi limitation with cycloheximide and proteasome inhibitor MG132 resulted in increased stability of EYFP: pdf2^{ΔST} and EYFP:gl2^{L480P} (Fig. 7c,d), consistent with the possibility that the START mutant proteins are degraded via the proteasome. Alternatively or additionally, it is possible that unknown components that normally destabilize START mutant proteins, are degraded via the proteasome. Taken together, these experiments reveal that the HD-Zip TFs PDF2 and GL2 are destabilized under Pi limitation, and that the START domain is critical for protein stability under both Pi sufficiency and limitation.

Discussion

HD-Zip protein PDF2 binds lysophospholipids via its START domain

The main finding herein is that PDF2, via its START domain, directly interacts with lysophosphatidylcholines (LysoPCs). Our initial strategy was to identify *in vivo* binding partners of this representative HD-Zip IV TF by performing TAP experiments with *Arabidopsis* cell lines. We followed up on lysophospholipids as candidate ligands using *in vitro* binding validation. Our data are consistent with a previous study in which START domains of PDF2, ATML1, and GL2 were expressed in yeast and subjected to immunoisolation (Schrick *et al.*, 2014). Subsequent lipidomic analysis revealed enrichment of LysoPCs and other phospholipids (PC and PS) in START domain pull-down samples (Schrick *et al.*, 2014). Although it is possible that the epidermal cells in which these TFs are predominantly expressed contain additional ligands, lysophospholipids now emerge as important PDF2 interactors.

LysoPC arises from partial hydrolysis of PC to remove one of the fatty acid groups. Since Pi starvation induces breakdown of PC in plants, LysoPCs serve as intermediates of the plastidic lipid biogenesis pathway. It was proposed *c*. 20 yr ago that LysoPC is exported from ER to chloroplast as a precursor for galactolipid synthesis (Mongrand *et al.*, 2000). Lysophospholipids are additionally thought to serve as messengers in plants. In arbuscular mycorrhizal symbiosis, roots use LysoPC as a signaling molecule to induce expression of endogenous Pi transporter genes (Drissner *et al.*, 2007). LysoPC is known to stimulate plasma

led from https://nph.onlinelibrary.wiley.com/doi/10.1111/nph.19917 by Kathrin Schrick

State University, Wiley Online Library on [02/07/2024]. See the Terms

) on Wiley Online Library for rules of use; OA articles are governed by the applicable Crea

membrane H⁺-ATPase activity (Palmgren *et al.*, 1988; Palmgren & Sommarin, 1989), which in turn provides the driving force for uptake of Pi in the root epidermis under Pi limitation (Yan

et al., 2002; Yuan et al., 2017). Interestingly, genetic analysis in *Medicago truncatula* indicates that H⁺-ATPase is required for Pi transport during arbuscular mycorrhizal symbiosis (Krajinski

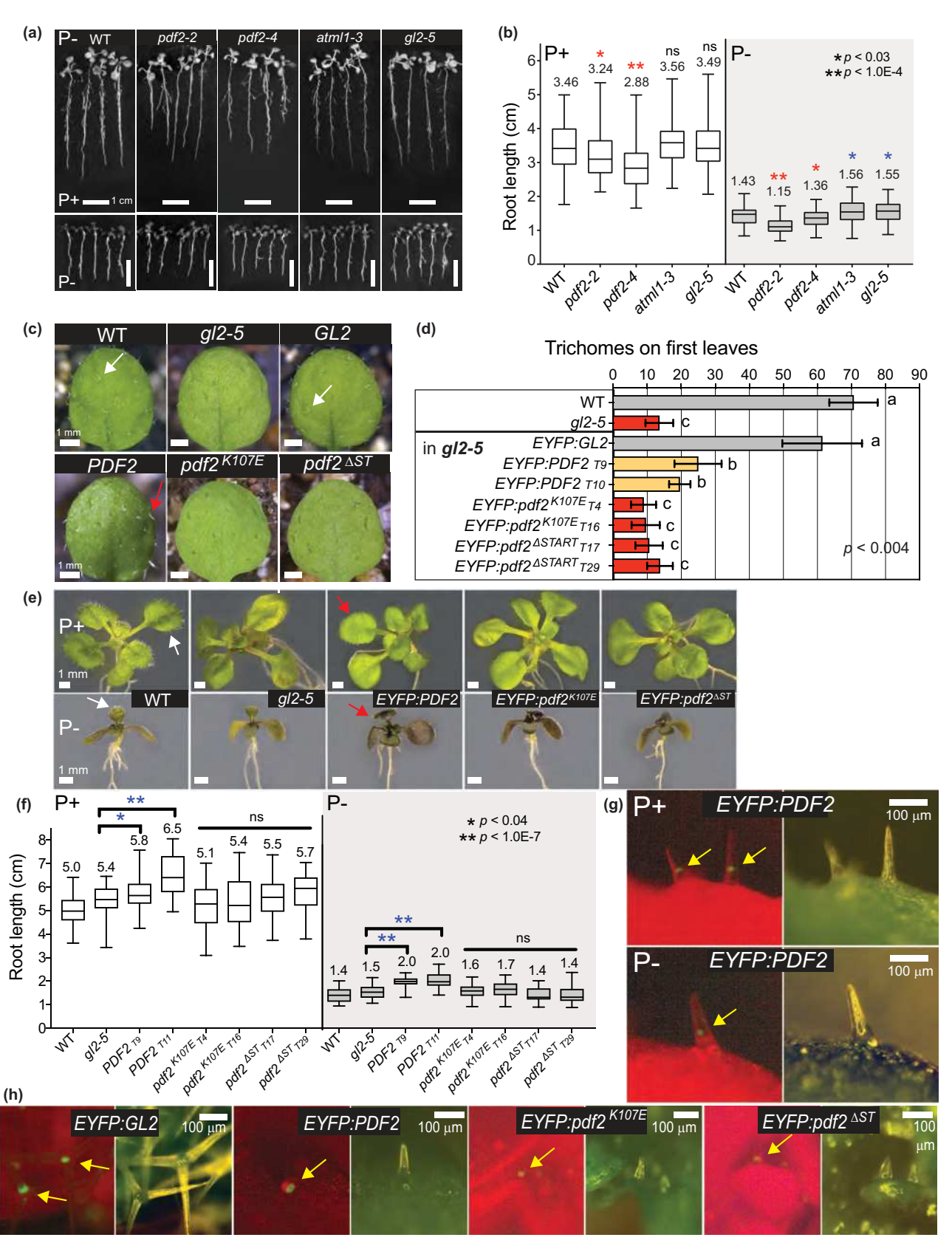


Fig. 5 START domain-dependent expression of *PDF2* drives elongation growth. (a) *Arabidopsis thaliana* seedlings from wild-type (WT), and HD-Zip IV mutants were grown under Pi sufficiency (P+) or limitation (P−) for 14 d. Bars, 1.0 cm. (b) Root lengths for seedlings from each genotype. Each box plot represents n > 70 seedlings from 2–5 independent experiments. Horizontal lines denote median. Whiskers indicate minimum and maximum values. Means are reported above box plots. Significant decreases (red) or increases (blue) from WT (unpaired t-test with Welch's correction): *, P < 0.03 or **, P < 0.0001. (c) Ectopic expression of PDF2 results in gain-of-function trichome phenotype that is HD and START domain-dependent. First leaves of WT and g/2-5 plants in comparison to proGL2:EYFP:DF2, proGL2:EYFP:DF2, $proGL2:EYFP:pdf2^{K107E}$ and $proGL2:EYFP:pdf2^{AST}$ in g/2-5 background. Arrows indicate normal (white) and abnormal (red) leaf trichomes. Bars, 1 mm. See also Supporting Information Fig. S7. (d) Quantification of leaf trichomes. Error bars indicate SD for $n \ge 20$ plants. Significant differences are marked by letters (unpaired t-test: *, P < 0.00001). (e) Phenotypes of 14-d-old seedlings under P+ or P− conditions. Arrows indicate normal (white) and abnormal (red) leaf trichomes. Bars, 1 mm. (f) Ectopic expression of PDF2 drives root elongation. Quantification of root lengths for seedlings shown in (e). Each box plot represents $n \ge 29$ seedlings from two independent experiments. Two independent transformants (T#) were analyzed for each transgene. Significant increases (blue) to control (unpaired t-test with Welch's correction): *, P < 0.04 or **, P < 1.0E-4. (g, h) Epifluorescence (left) with matching light images (right) of leaf trichomes from 14-d-old seedlings. Bars, 100 µm. (g) EYFP:PDF2 is nuclear localized under P+ and P− conditions (arrows). (h) EYFP-tagged WT and mutant proteins are nuclear localized (arrows).

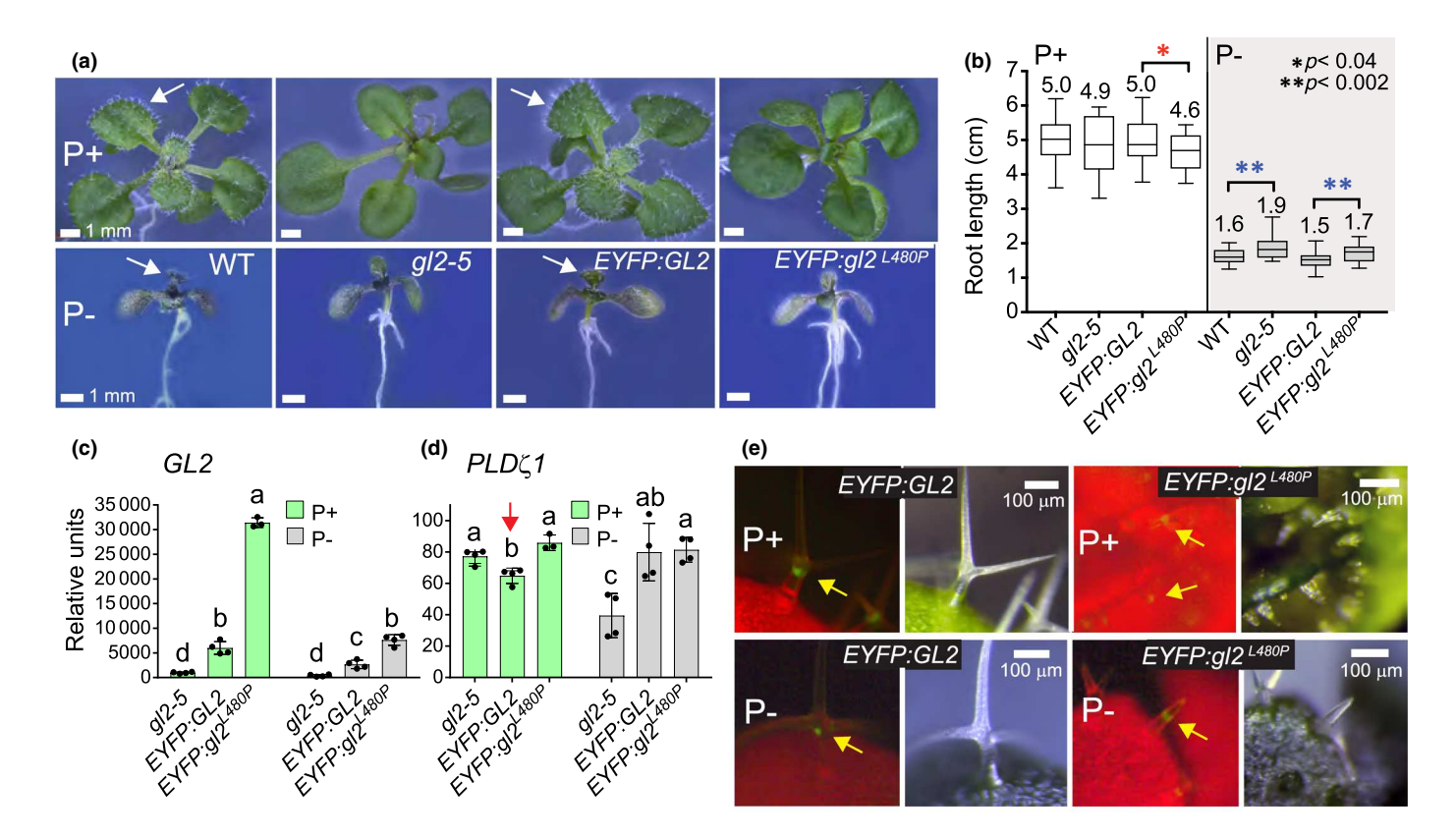


Fig. 6 START mutant L480P affects root elongation and target gene repression of GL2. (a) Phenotypes of 14-d-old Arabidopsis thaliana seedlings from wild-type (WT), g/2-5, proGL2:EYFP:GL2 and proGL2:EYFP: $g/2^{L480P}$ (in g/2-5 background) under Pi sufficiency (P+) or limitation (P−). Normal leaf trichomes (arrows). Bars, 1 mm. (b) Root lengths for $n \ge 21$ seedlings. Horizontal lines in box plots denote median, and whiskers indicate minimum and maximum values. Significant decrease (red) or increase (blue) to control (unpaired t-test with Welch's correction): *, P < 0.04 or **, P < 0.002. (c, d) Quantitative real-time polymerase chain reaction with cDNA from 14-d-old seedling shoots under P+ or P− conditions, normalized to reference gene ACT7. (c) The GL2/g/2 mRNA is expressed in both WT EYFP:GL2 and mutant EYFP: $g/2^{L480P}$ lines. (d) The transcriptional target gene $PLD\zeta 1$ is repressed by EYFP:GL2 (arrow) but not EYFP: $g/2^{L480P}$ under P+ conditions. Significant differences between genotypes determined by one-way ANOVA, Tukey's test, and indicated by letters: P < 0.05. (e) Epifluorescence (left) with matching light images (right) of leaf trichomes from 14-d-old seedlings. EYFP:GL2 and EYFP:

et al., 2014). In Arabidopsis, extracellular LysoPC is taken up by an ATPase flippase in the root epidermis, and it is speculated that the detection of LysoPC signals the availability of Pi in the decaying humus in soils (Poulsen et al., 2015). Our study raises the possibility that the internalization of LysoPCs activates not only plasma membrane H⁺-ATPase, but also elicits a transcriptional response by binding to the START domain of PDF2.

PDF2 START domain binding to LysoPCs in *Arabidopsis* cells (Fig. 1), in yeast (Schrick *et al.*, 2014), and *in vitro* (Fig. 2f) builds on mounting evidence that links HD-Zip IV TFs with phospholipid sensing. In 2003, GL2 was identified as a negative regulator of phospholipase D (*PLD*\(\zeta\)1) in root hair patterning (Ohashi *et al.*, 2003). Further insights came from studies with mammalian STARD2/PC transfer protein

ded from https://nph.onlinelibrary.wiley.com/doi/10.1111/nph.19917 by Kathrin Schrick

- Kansas State University, Wiley Online Library on [02/07/2024]. See the Terms

) on Wiley Online Library for rules of use; OA articles are governed by the applicable Crea

(PCTP), which binds PC and is expressed during embryonic development in the mouse. STARD2/PCTP interacts with and enhances TF activity of Pax3, a mammalian HD protein (Kanno *et al.*, 2007). The START domain from human

PCTP, similarly to the PDF2 START domain, also recruits LysoPCs in pull-down experiments in yeast (Schrick *et al.*, 2014). Our findings introduce the intriguing possibility that START-dependent mechanisms linking Pi sensing and

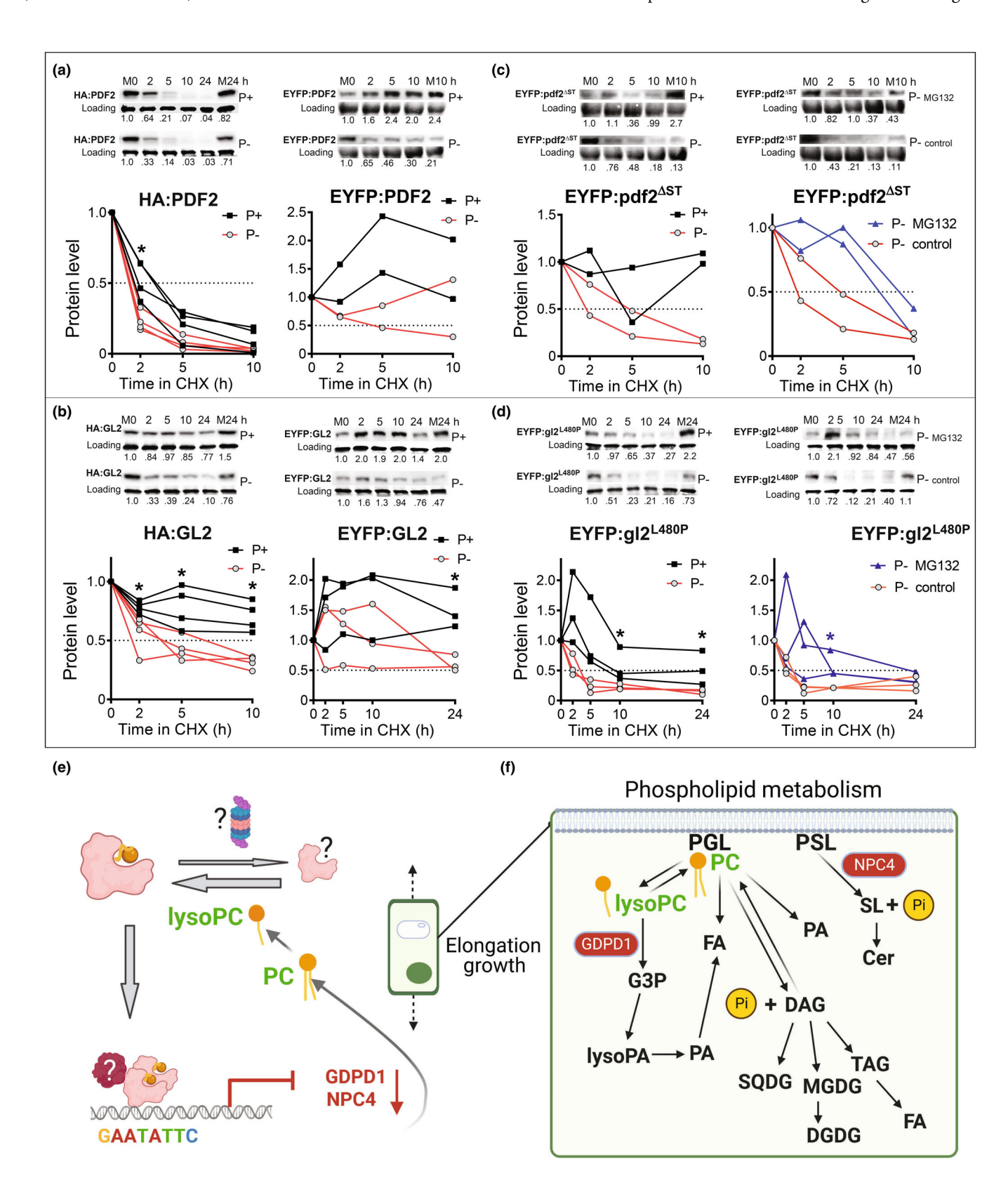


Fig. 7 Protein stability of GL2 and PDF2 depends on Pi status and START domain: Model for PDF2 as a lipid sensor. (a-d) Arabidopsis thaliana seedlings were grown on P+ or P- media for 5-6 d before cycloheximide (400 μM) treatment for 10 or 24 h. Western blot with anti-HA or -GFP antibodies, followed by Coomassie blue staining for loading controls. M0 and M10 (or M24), DMSO mock treatments at 0 and 10 (or 24 h). Each blot is representative of n = 3-4 independent experiments, except for EYFP:PDF2 and EYFP:pdf2^{Δ ST}, which represent n = 2 independent experiments. Both biological replicates of EYFP:pdf2^{AST} (P – media) are shown. See Supporting Information Fig. S7 for other replicates. Protein quantification, with values normalized to MO, is graphed beneath western blots. Intersection with dotted line (0.5) denotes protein half-life. Significant differences (unpaired t-test): *, P \leq 0.05. (a, b) Protein stability of PDF2 and GL2 is reduced under Pi limitation, regardless of epitope tag. Both (a) HA:PDF2 and EYFP:PDF2 and (b) HA: GL2 and EYFP:GL2 proteins display shorter half-lives under Pi limitation. (c, d) Protein instability of START domain mutants is further reduced under Pi limitation. Under Pi sufficiency, the (c) pdf2^{AST} and (d) gl2^{L480P} mutants exhibit a shorter half-life in comparison to the wild-type proteins, and this instability is enhanced by Pi limitation. Proteasome inhibitor MG132 (50 μ M) treatment partially restores the stability of (c) pdf2 $^{\Delta ST}$ and (d) gl2 L480P mutant proteins under Pi limitation. (e) Model: PDF2 is a lipid sensor. The START domain of PDF2 binds a lipid ligand, resulting in either stabilization (thick gray arrows) or destabilization (thin gray arrow) of the protein, possibly via the proteasome. In the illustrated scenario, LysoPC binding results in stabilized TF that dimerizes and binds to the P1BS palindrome upstream of phospholipid catabolic genes. Transcriptional repression (blunt ended arrow) occurs through interaction with an unknown corepressor. Gene regulation drives the maintenance of membrane phospholipids (black arrows) in epidermal cells undergoing elongation growth (dashed line arrows), even under Pi limitation. (f) LysoPC plays a central role in phospholipid catabolism. Phosphoglycerolipids (PGL) and phosphosphingolipids (PSL) of the plasma membrane are major stores of Pi in the cell. The GDPD and NPC4 enzymatic steps are transcriptionally repressed by PDF2. These events result in phospholipid accumulation and production of LysoPC, which in turn binds PDF2 to positively regulate its activity (a). Black arrows indicate directions of enzymatic steps. This figure was created with BioRender.com.

transcriptional control of phospholipid metabolism are conserved across organisms.

Dual role of PDF2 as a metabolic sensor and transcriptional regulator of phospholipid catabolism and Pi-induced starvation

Here we identify PDF2 as a negative regulator of two phospholipid catabolism genes, *GDPD1* and *NPC4*. Until now, PDF2 was viewed primarily as an activator that functions redundantly with ATML1 to upregulate L1 genes. Surprisingly, the DAP-seq data identified a P1BS palindrome (GAATATTC) as the main DNA-binding motif for PDF2 (Fig. 3a), as opposed to the L1 box (TAAATCTA), which was reported as the DNA-binding motif for both ATML1 and PDF2 (Rombola-Caldentey *et al.*, 2014).

Our gene expression studies show that *pdf2*, and not *atml1* mutants exhibit transcriptional upregulation of *GDPD1* and *SPX1*, suggesting that PDF2 is the main repressor of these genes in the shoot. Moreover, ectopic *PDF2* expression that was dependent on the START domain was sufficient to drive repression of three genes, namely *GDPD1*, *SPX1* and *NPC4* (Fig. 3l). The other gene targets that we selected for quantitative real-time polymerase chain reaction analysis showed inconsistencies in mRNA expression, suggesting complex gene regulatory networks with respect to *PDF2* function at the seedling stage. Thus, it would be interesting to investigate how *PDF2* affects genome-wide mRNA expression of the DAP-seq predicted transcriptional targets at multiple developmental stages.

Model for PDF2 as a lipid sensor

We propose that PDF2 functions as a lipid sensor for phospholipids via its START domain (Fig. 7e). In one possible model, LysoPCs bind to START to stabilize the protein, resulting in transcriptional activity. PDF2 directly binds to the promoters of several phospholipid catabolism genes resulting in repression of phospholipid catabolism. Thereby, PDF2 activity promotes incorporation of phospholipids into membranes, driving elongation growth. Mutant analysis suggests that PDF2 is important for

fine-tuning transcript levels of phospholipid catabolic genes (Fig. 3). Under Pi starvation, overall phospholipid levels including LysoPCs decrease, resulting in reduced PDF2 protein levels and reduced cell elongation. However, PDF2 levels are not completely abolished. According to this model, the transcriptional activity of PDF2 is critical to regulate phospholipid catabolic genes to allow measured elongation growth according to lysophospholipid levels. Under Pi limitation, we suggest that a pool of PDF2 protein is bound to a destabilizing ligand or unliganded, resulting in degradation that could in part be regulated by the proteasome and components that remain to be identified.

PDF2 activity is positioned to protect membrane lipid biogenesis in the epidermis when Pi is limiting. Derepression of phospholipid catabolic genes leads to the production of fatty acids, galactolipids, as well as DAG and TAG, and recycling back to phospholipids (Fig. 7f). Our lipidomic profiling of pdf2, atml1, and gl2 mutants uncovered altered levels of several types of phospholipids, as well as products of phospholipid catabolism. While pdf2 mutants exhibited elongation defects in the seedling, we found that ectopic expression of PDF2 drives root elongation. The growth promoting activity in the seedling requires the function of both the START domain and HD (Fig. 5f). By contrast, ectopic expression of EYFP:PDF2 (or EYFP:ATML1) under the GL2 epidermis-specific promoter leads to dwarfism in adult plants (Fig. S7), a phenotype that is abolished by HD or START domain mutation. These observations highlight the importance of PDF2 in maintaining the normal growth pattern. We also noted that in comparison to PDF2, mutations in GL2 had opposite effects on root elongation depending on Pi availability (Fig. 6b), suggesting further complexities underlying the function of HD-Zip IV proteins in growth regulation.

Why should a phospholipid sensing mechanism that transcriptionally controls phospholipid catabolism function in the epidermis? In addition to its myriad protective functions, the epidermis plays a critical role in controlling growth. The brassinosteroid pathway for cell expansion and cell division is required in the L1 layer (Savaldi-Goldstein *et al.*, 2007), and epidermis-localized VLCFA biosynthesis is implicated in growth control (Nobusawa *et al.*, 2013). Here we show that PDF2 negatively regulates

GDPD1 (Fig. 3), which encodes an enzyme that hydrolyzes glycerophosphodiesters to glycerol-3-phosphate to control phospholipid homeostasis (Cheng et al., 2011). We identified another PDF2 target gene, NPC4 (Fig. 3), that is important for hydrolysis and breakdown of glycosyl inositol phosphoceramides (GIPC) (Yang et al., 2021). These phosphosphingolipids, along with phosphoglycerolipids, are major constituents of the plasma membrane. It is estimated that in plants, about one-third of cellular Pi is stored in membrane phospholipids. Our study highlights the importance of membrane phospholipids and lipid homeostasis as a regulator of growth in the epidermis.

Perspectives on START domains as phospholipid sensors

Whether other START domain-containing HD-Zip TFs besides PDF2 bind lysophospholipids needs to be tested experimentally. Considering that mammalian START proteins differ in their specificity toward various lipids ranging from fatty acids to sterols, a similar diversification is expected in plants. VLCFA-ceramides were proposed to bind the START domain of ATML1 and PDF2 in maintaining epidermal specificity (Nagata et al., 2021; Nagata & Abe, 2023). Fitting with this possibility, our TAP results for PDF2 identified one ceramide species (Cer t18:1/c24:0) that is enriched in WT vs the pdf2^{ASTART} mutant (Fig. 1e). In vitro studies suggest that a HD-Zip III TF binds PC and other phospholipids through its START domain (Husbands et al., 2023). Aside from HD-Zip III and IV TFs, Arabidopsis contains 14 START proteins whose ligands are unknown (Schrick et al., 2004). The START domain-containing wheat stripe rust resistance protein WKS1 shows specificity toward phosphatidic acid and phosphatidylinositol phosphates in protein lipid overlay assays (Gou et al., 2015). Another START protein from Marchantia was implicated in lipid transfer activity during Pi deprivation (Hirashima et al., 2021).

It is noteworthy that this newly discovered lipid metabolism connection between PDF2 and lysophospholipids relates to sensing of Pi, a nutrient that is crucial for plant growth. Our findings open a new area of research that will further explore how Pi sensing and membrane lipid metabolism are integrated with the developmental program in plants and across multicellular organisms. Intriguingly, a human START protein of the thioesterase family (THEM1/STARD14) that is critical for brown fat metabolism is allosterically regulated via its binding to LysoPC and fatty acids (Tillman *et al.*, 2020). Since both LysoPCs and fatty acids are breakdown products of membrane lipid catabolism in plants, future investigations will explore how START domains evolved to effectively orchestrate gene expression networks according to environmentally guided metabolic inputs.

Accession numbers

Arabidopsis thaliana HD-Zip IV TFs: PDF2 (At4g04890), GL2 (At1g79840), ATML1 (At4g21750); Physcomitrium patens HD-Zip IV TF: PpHDZIV (XP_024401280.1), Homo sapiens START domain proteins: StAR/STARD1 (NP_000340.2); Homo sapiens

PCTP/STARD2 (NP_067036.2); *Arabidopsis thaliana* phospholipid catabolism enzymes: GDPD1 (At3g02040), GDPD2 (At5g41080), GDPD3 (At5g43300), NPC2 (At2g26870), NPC4 (At3g03530), NPC6 (At3g48610), PLA2 β (At2g19690); PLD ϵ (At1g55180), PLD ζ 1 (At3g16785), PLD ζ 2 (At3g05630); Other Pi starvation-related proteins: PHO1 (At3g23430), PHO1;H1 (At1g68740), SPX1 (At5g20150).

Acknowledgements

This research was funded by the National Science Foundation (MCB1616818), National Institute of General Medical Sciences of the National Institute of Health under Award no. P20GM103418, USDA National Institute of Food and Agriculture Hatch/Multi-State project 1013013, and Johnson Cancer Research Center at Kansas State University to KS and the National Science Foundation grant 2226270 to AS. This is contribution no. 20-003-J from the Kansas Agricultural Experiment Station. We thank Anne Michaelis for processing lipidomics samples, Mary Roth for help with lipid extraction, and Adrienne Roeder, Xuemin Wang, Ruth Welti and Lothar Willmitzer for valuable input.

Competing interests

None declared.

Author contributions

IW, AS and KS conceived of the experiments and wrote the manuscript. XH and AK designed and developed constructs for recombinant expression in *E. coli.* KS, GLM and AAP performed RNA extractions and quantitative real-time polymerase chain reaction and GLM analyzed DAP-seq data. IW and JS performed TAP experiments and analyzed data. IW purified recombinant protein and AS performed liposome binding experiments. KS prepared protein alignment and structural models. PK-B, AT, DKH and AS prepared liposomes. KS, AK, TM, KAT and STP designed and constructed plasmids for DNA binding and plant assays. TM and BA performed DNA-binding assays. KS and TM performed lipid extractions. KS and BS performed cycloheximide assays. STP and KS conducted root growth assays and EYFP expression analysis, and KS performed trichome quantification.

ORCID

Data availability

The data that supports the findings of this study are available in the Supporting Information of this article.

References

- Abe M, Katsumata H, Komeda Y, Takahashi T. 2003. Regulation of shoot epidermal cell differentiation by a pair of homeodomain proteins in Arabidopsis. *Development* 130: 635–643.
- Alpy F, Legueux F, Bianchetti L, Tomasetto C. 2009. START domaincontaining proteins: a review of their role in lipid transport and exchange. *Medical Science* 25: 181–191.
- Alpy F, Tomasetto C. 2005. Give lipids a START: the StAR-related lipid transfer (START) domain in mammals. *Journal of Cell Science* 118(Pt 13): 2791–2801.
- Bose HS, Sugawara T, Strauss JF 3rd, Miller WL, International Congenital Lipoid Adrenal Hyperplasia Consortium. 1996. The pathophysiology and genetics of congenital lipoid adrenal hyperplasia. *The New England Journal of Medicine* 335: 1870–1878.
- Cheng Y, Zhou W, El Sheery NI, Peters C, Li M, Wang X, Huang J. 2011. Characterization of the Arabidopsis glycerophosphodiester phosphodiesterase (GDPD) family reveals a role of the plastid-localized AtGDPD1 in maintaining cellular phosphate homeostasis under phosphate starvation. *The Plant Journal* 66: 781–795.
- Clark BJ. 2020. The START-domain proteins in intracellular lipid transport and beyond. Molecular and Cellular Endocrinology 504: 110704.
- Clough SJ, Bent AF. 1998. Floral dip: a simplified method for Agrobacteriummediated transformation of Arabidopsis thaliana. The Plant Journal 1: 735–743.
- Drissner D, Kunze G, Callewaert N, Gehrig P, Tamasloukht M, Boller T, Felix G, Amrhein N, Bucher M. 2007. Lyso-phosphatidylcholine is a signal in the arbuscular mycorrhizal symbiosis. *Science* 318: 265–268.
- Earley KW, Haag JR, Pontes O, Opper K, Juehne T, Song K, Pikaard CS. 2006. Gateway-compatible vectors for plant functional genomics and proteomics. *The Plant Journal* 45: 616–629.
- Fluck CE, Maret A, Mallet D, Portrat-Doyen S, Achermann JC, Leheup B, Theintz GE, Mullis PE, Morel Y. 2005. A novel mutation L260P of the steroidogenic acute regulatory protein gene in three unrelated patients of Swiss ancestry with congenital lipoid adrenal hyperplasia. *The Journal of Clinical Endocrinology and Metabolism* 90: 5304–5308.
- Giavalisco P, Li Y, Matthes A, Eckhardt A, Hubberten HM, Hesse H, Segu S, Hummel J, Kohl K, Willmitzer L. 2011. Elemental formula annotation of polar and lipophilic metabolites using (13) C, (15) N and (34) S isotope labelling, in combination with high-resolution mass spectrometry. *The Plant Journal* 68: 364–376.
- Gou JY, Li K, Wu K, Wang X, Lin H, Cantu D, Uauy C, Dobon-Alonso A, Midorikawa T, Inoue K et al. 2015. Wheat stripe rust resistance protein WKS1 reduces the ability of the thylakoid-associated ascorbate peroxidase to detoxify reactive oxygen species. Plant Cell 27: 1755–1770.
- Hirashima T, Jimbo H, Kobayashi K, Wada H. 2021. A START domaincontaining protein is involved in the incorporation of ER-derived fatty acids into chloroplast glycolipids in *Marchantia polymorpha*. *Biochemical and Biophysical Research Communications* 534: 436–441.
- Husbands AY, Feller A, Aggarwal V, Dresden CE, Holub AS, Ha T, Timmermans MCP. 2023. The START domain potentiates HD-ZIPIII transcriptional activity. *Plant Cell* 35: 2332–2348.
- Kamata N, Okada H, Komeda Y, Takahashi T. 2013a. Mutations in epidermisspecific HD-ZIP IV genes affect floral organ identity in *Arabidopsis thaliana*. *The Plant Journal* 75: 430–440.
- Kamata N, Sugihara A, Komeda Y, Takahashi T. 2013b. Allele-specific effects of PDF2 on floral morphology in *Arabidopsis thaliana*. *Plant Signaling & Behavior* 8: e27417.
- Kanno K, Wu MK, Agate DS, Fanelli BJ, Wagle N, Scapa EF, Ukomadu C, Cohen DE. 2007. Interacting proteins dictate function of the minimal START domain phosphatidylcholine transfer protein/StarD2. The Journal of Biological Chemistry 282: 30728–30736.

- Khosla A, Paper JM, Boehler AP, Bradley AM, Neumann TR, Schrick K. 2014. HD-Zip proteins GL2 and HDG11 have redundant functions in Arabidopsis trichomes, and GL2 activates a positive feedback loop via MYB23. *Plant Cell* 26: 2184–2200
- Krajinski F, Courty PE, Sieh D, Franken P, Zhang H, Bucher M, Gerlach N, Kryvoruchko I, Zoeller D, Udvardi M et al. 2014. The H+-ATPase HA1 of Medicago truncatula is essential for phosphate transport and plant growth during arbuscular mycorrhizal symbiosis. Plant Cell 26: 1808–1817.
- Letourneau D, Lefebvre A, Lavigne P, LeHoux JG. 2015. The binding site specificity of STARD4 subfamily: breaking the cholesterol paradigm. *Molecular and Cellular Endocrinology* 408: 53–61.
- Letourneau D, Lorin A, Lefebvre A, Frappier V, Gaudreault F, Najmanovich R, Lavigne P, LeHoux JG. 2012. StAR-related lipid transfer domain protein 5 binds primary bile acids. *Journal of Lipid Research* 53: 2677–2689.
- Li M, Welti R, Wang X. 2006. Quantitative profiling of Arabidopsis polar glycerolipids in response to phosphorus starvation. Roles of phospholipases D zeta1 and D zeta2 in phosphatidylcholine hydrolysis and digalactosyldiacylglycerol accumulation in phosphorus-starved plants. *Plant Physiology* 142: 750–761.
- Lin WD, Liao YY, Yang TJ, Pan CY, Buckhout TJ, Schmidt W. 2011.
 Coexpression-based clustering of Arabidopsis root genes predicts functional modules in early phosphate deficiency signaling. *Plant Physiology* 155: 1383–1402.
- Luzarowski M, Kosmacz M, Sokolowska E, Jasinska W, Willmitzer L, Veyel D, Skirycz A. 2017. Affinity purification with metabolomic and proteomic analysis unravels diverse roles of nucleoside diphosphate kinases. *Journal of Experimental Botany* 68: 3487–3499.
- Luzarowski M, Wojciechowska I, Skirycz A. 2018. 2 in 1: one-step affinity purification for the parallel analysis of protein-protein and protein-metabolite complexes. *Journal of Visualized Experiments* 138: 57720.
- Mi HY, Muruganujan A, Ebert D, Huang XS, Thomas PD. 2019. PANTHER version 14: more genomes, a new PANTHER GO-slim and improvements in enrichment analysis tools. *Nucleic Acids Research* 47: D419–D426.
- Mongrand S, Cassagne C, Bessoule JJ. 2000. Import of lyso-phosphatidylcholine into chloroplasts likely at the origin of eukaryotic plastidial lipids. *Plant Physiology* 122: 845–852.
- Mukherjee T, Subedi B, Khosla A, Begler EM, Stephens PM, Warner AL, Lerma-Reyes R, Thompson KA, Gunewardena S, Schrick K. 2022. The START domain mediates Arabidopsis GLABRA2 dimerization and turnover independently of homeodomain DNA binding. *Plant Physiology* 190: 2315–2334.
- Murashige T, Skoog F. 1962. A revised medium for rapid growth and bio assays with tobacco tissue cultures. *Physiologia Plantarum* 15: 473–497.
- Nagata K, Abe M. 2023. A conserved mechanism determines the activity of two pivotal transcription factors that control epidermal cell differentiation in *Arabidopsis thaliana*. *Journal of Plant Research* 136: 349–358.
- Nagata K, Ishikawa T, Kawai-Yamada M, Takahashi T, Abe M. 2021.
 Ceramides mediate positional signals in *Arabidopsis thaliana* protoderm differentiation. *Development* 148: dev194969.
- Nakamura Y, Awai K, Masuda T, Yoshioka Y, Takamiya K, Ohta H. 2005. A novel phosphatidylcholine-hydrolyzing phospholipase C induced by phosphate starvation in Arabidopsis. *Journal of Biological Chemistry* 280: 7469–7476.
- Nobusawa T, Okushima Y, Nagata N, Kojima M, Sakakibara H, Umeda M. 2013. Synthesis of very-long-chain fatty acids in the epidermis controls plant organ growth by restricting cell proliferation. *PLoS Biology* 11: e1001531.
- Ogawa E, Yamada Y, Sezaki N, Kosaka S, Kondo H, Kamata N, Abe M, Komeda Y, Takahashi T. 2015. ATML1 and PDF2 play a redundant and essential role in Arabidopsis embryo development. *Plant & Cell Physiology* 56: 1183–1192.
- Ohashi Y, Oka A, Rodrigues-Pousada R, Possenti M, Ruberti I, Morelli G, Aoyama T. 2003. Modulation of phospholipid signaling by GLABRA2 in root-hair pattern formation. *Science* 300: 1427–1430.
- O'Malley RC, Huang SC, Song L, Lewsey MG, Bartlett A, Nery JR, Galli M, Gallavotti A, Ecker JR. 2016. Cistrome and epicistrome features shape the regulatory DNA landscape. *Cell* 165: 1280–1293.

- Palmgren MG, Sommarin M. 1989. Lysophosphatidylcholine stimulates ATP dependent proton accumulation in isolated oat root plasma membrane vesicles. *Plant Physiology* 90: 1009–1014.
- Palmgren MG, Sommarin M, Ulvlskov P, Jorgensen PL. 1988. Modulation of plasma membrane H+-ATPase from oat roots by lysophophatidylcholine, free fatty acids and phospholipase A₂. *Physiologia Plantarum* 74: 11–19.
- Pant BD, Burgos A, Pant P, Cuadros-Inostroza A, Willmitzer L, Scheible WR. 2015. The transcription factor PHR1 regulates lipid remodeling and triacylglycerol accumulation in *Arabidopsis thaliana* during phosphorus starvation. *Journal of Experimental Botany* 66: 1907–1918.
- Peterson KM, Shyu C, Burr CA, Horst RJ, Kanaoka MM, Omae M, Sato Y, Torii KU. 2013. Arabidopsis homeodomain-leucine zipper IV proteins promote stomatal development and ectopically induce stomata beyond the epidermis. *Development* 140: 1924–1935.
- Ponting CP, Aravind L. 1999. START: a lipid-binding domain in StAR, HD-ZIP and signalling proteins. *Trends in Biochemical Sciences* 24: 130–132.
- Poulsen LR, Lopez-Marques RL, Pedas PR, McDowell SC, Brown E, Kunze R, Harper JF, Pomorski TG, Palmgren M. 2015. A phospholipid uptake system in the model plant *Arabidopsis thaliana*. *Nature Communications* 6: 7649.
- Puga MI, Mateos I, Charukesi R, Wang Z, Franco-Zorrilla JM, de Lorenzo L, Irigoyen ML, Masiero S, Bustos R, Rodriguez J et al. 2014. SPX1 is a phosphate-dependent inhibitor of Phosphate Starvation Response 1 in Arabidopsis. Proceedings of the National Academy of Sciences, USA 111: 14947– 14952.
- Roderick SL, Chan WW, Agate DS, Olsen LR, Vetting MW, Rajashankar KR, Cohen DE. 2002. Structure of human phosphatidylcholine transfer protein in complex with its ligand. *Nature Structural Biology* 9: 507–511.
- Roeder AH, Cunha A, Ohno CK, Meyerowitz EM. 2012. Cell cycle regulates cell type in the Arabidopsis sepal. *Development* 139: 4416–4427.
- Rombola-Caldentey B, Rueda-Romero P, Iglesias-Fernandez R, Carbonero P, Onate-Sanchez L. 2014. Arabidopsis DELLA and two HD-ZIP transcription factors regulate GA signaling in the epidermis through the L1 box *cis*-element. *Plant Cell* 26: 2905–2919.
- Roy A, Kucukural A, Zhang Y. 2010. I-TASSER: a unified platform for automated protein structure and function prediction. *Nature Protocols* 5: 725– 738.
- Rubio V, Linhares F, Solano R, Martin AC, Iglesias J, Leyva A, Paz-Ares J. 2001. A conserved MYB transcription factor involved in phosphate starvation signaling both in vascular plants and in unicellular algae. *Genes & Development* 15: 2122–2133.
- San-Bento R, Farcot E, Galletti R, Creff A, Ingram G. 2014. Epidermal identity is maintained by cell-cell communication via a universally active feedback loop in Arabidopsis thaliana. *The Plant Journal* 77: 46–58.
- Savaldi-Goldstein S, Peto C, Chory J. 2007. The epidermis both drives and restricts plant shoot growth. *Nature* 446: 199–202.
- Schrick K, Bruno M, Khosla A, Cox PN, Marlatt SA, Roque RA, Nguyen HC, He C, Snyder MP, Singh D et al. 2014. Shared functions of plant and mammalian StAR-related lipid transfer (START) domains in modulating transcription factor activity. BMC Biology 12: 70.
- Schrick K, Nguyen D, Karlowski WM, Mayer KF. 2004. START lipid/sterolbinding domains are amplified in plants and are predominantly associated with homeodomain transcription factors. *Genome Biology* 5: R41.
- Scott SP, Teh A, Peng C, Lavin MF. 2002. One-step site-directed mutagenesis of ATM cDNA in large (20kb) plasmid constructs. *Human Mutation* 20: 323.
- Sluchanko NN, Tugaeva KV, Faletrov YV, Levitsky DI. 2016. High-yield soluble expression, purification and characterization of human steroidogenic acute regulatory protein (StAR) fused to a cleavable Maltose-Binding Protein (MBP). Protein Expression and Purification 119: 27–35.
- Subedi B, Schrick K. 2022. EYFP fusions to HD-Zip IV transcription factors enhance their stability and lead to phenotypic changes in Arabidopsis. *Plant Signaling & Behavior* 17: 2119013.
- Takada S, Takada N, Yoshida A. 2013. ATML1 promotes epidermal cell differentiation in Arabidopsis shoots. *Development* 140: 1919–1923.
- Tillman MC, Imai N, Li Y, Khadka M, Okafor CD, Juneja P, Adhiyaman A, Hagen SJ, Cohen DE, Ortlund EA. 2020. Allosteric regulation of thioesterase superfamily member 1 by lipid sensor domain binding fatty acids and

- lysophosphatidylcholine. *Proceedings of the National Academy of Sciences, USA* 117: 22080–22089.
- Van Leene J, Eeckhout D, Persiau G, Van De Slijke E, Geerinck J, Van Isterdael G, Witters E, De Jaeger G. 2011. Isolation of transcription factor complexes from Arabidopsis cell suspension cultures by tandem affinity purification. Methods in Molecular Biology 754: 195–218.
- Yan F, Zhu Y, Muller C, Zorb C, Schubert S. 2002. Adaptation of H+-pumping and plasma membrane H+ ATPase activity in proteoid roots of white lupin under phosphate deficiency. *Plant Physiology* 129: 50–63.
- Yang B, Li M, Phillips A, Li L, Ali U, Li Q, Lu S, Hong Y, Wang X, Guo L. 2021. Nonspecific phospholipase C4 hydrolyzes phosphosphingolipids and sustains plant root growth during phosphate deficiency. *Plant Cell* 33: 766–780.
- Yang J, Zhang Y. 2015. I-TASSER server: new development for protein structure and function predictions. *Nucleic Acids Research* 43(W1): W174–W181.
- Yuan W, Zhang D, Song T, Xu F, Lin S, Xu W, Li Q, Zhu Y, Liang J, Zhang J. 2017. Arabidopsis plasma membrane H+-ATPase genes AHA2 and AHA7 have distinct and overlapping roles in the modulation of root tip H+ efflux in response to low-phosphorus stress. *Journal of Experimental Botany* 68: 1731–1741.

Supporting Information

Additional Supporting Information may be found online in the Supporting Information section at the end of the article.

- **Dataset S1** Lipidomics mass spectrometry details: all detected peaks, putative metabolite name identified: tandem affinity purification experiment; mutants experiment; Pi limitation experiment.
- **Dataset S2** TAP lipidomics data for the PDF2 TF from soluble fractions.
- **Dataset S3** List of putative transcriptional target genes from DAP-seq data for PDF2 and GO enrichment for DAP-seq targets of PDF2.
- **Dataset S4** Comprehensive lipidomic data from wild-type and *pdf2*, *atml1*; *pdf2*, *atml1*, and *gl2* mutants and maximum normalized comprehensive lipidomic data from wild-type and *pdf2*, *atml1*; *pdf2*, *atml1*, and *gl2* mutants.
- **Dataset S5** Lipidomic data from wild-type, *pdf2*, *atml1*, and *gl2* mutants, as well as *EYFP:PDF2*, *EYFP:pdf2*^{ΔST}, *EYFP:GL2*, and *EYFP:gl2*^{ΔST} transgenic lines in Pi sufficient (P+) and Pi limiting (P-) media.
- **Fig. S1** Lysophosphatidylcholines bind to the START domain of PDF2 *in vitro*.
- Fig. S2 Putative transcriptional targets of PDF2 from DAP-seq data.
- **Fig. S3** The *atml1-1;pdf2-1* double mutant exhibits a severely altered lipid composition.
- **Fig. S4** Heat maps illustrate lipidomic profiles in wild type, *pdf2*, *atml1* and *gl2* seedling shoots under normal growth conditions.

- **Fig. S5** Lipid profiles for ceramides, galactolipids, and diacyland triacylglycerols in wild type, and *pdf2*, *atml1* and *gl2* mutants under Pi sufficiency and limitation.
- **Fig. S6** Heat maps illustrate lipidomic profiles in wild type, and *pdf2*, *atml1* and *gl2* mutants under Pi sufficiency and limitation.
- **Fig. S7** Plant phenotypes from START domain-dependent expression of *PDF2*.
- **Fig. S8** Protein stability of PDF2 and GL2 is reduced under Pi limitation and START domain mutants exhibit enhanced protein instability.
- **Table S1** Oligonucleotides used in this study.
- **Table S2** Lipidomic changes in *atml1;pdf2-1* vs wild-type *Arabidopsis thaliana* seedling apices.

- **Table S3** Lipidomic changes in *pdf2-1* vs wild-type *Arabidopsis thaliana* seedling apices under Pi limitation.
- **Table S4** Lipidomic changes in *pdf2-2* vs wild-type *Arabidopsis thaliana* seedling apices under Pi limitation.
- **Table S5** Lipidomic changes in *EYFP:pdf2*^{ΔSTART} vs *EYFP: PDF2 Arabidopsis thaliana* seedling apices under Pi limitation.

Please note: Wiley is not responsible for the content or functionality of any Supporting Information supplied by the authors. Any queries (other than missing material) should be directed to the *New Phytologist* Central Office.